

2017/07/03

Dear Editor,

We would like to express our sincere thanks for serving as the editor for our work.

We would like to inform you that we have revised the manuscript significantly based on the comments by the two reviewers. New interpretation and analysis along with some new figures have been done to answer the questions raised by the reviewers. The “Introduction” section has been shortened based on the suggestions from one of the reviewer. At the same time, the purpose behind incorporating the model in our study has also been defined clearly.

We, at this stage, strongly believe that the quality of the manuscript has improved and look forward to hearing positive result from your side.

Sincerely Yours,

Dipesh Rupakheti and Prof. Shichang Kang, on behalf of all coauthors

Pre-monsoon air quality over Lumbini, a world heritage site along the Himalayan foothills

by D. Rupakheti et al.

Review of Rupakheti et al. (Report #1, Anonymous Referee #4)

The authors present PM, BC, CO and O₃ concentrations measured at Lumbini during April-June 2013 and explained meteorology, pollutant concentrations by conducting WRF-Stem model simulation. They also estimated the regional contributions of CO and aerosol composition to local air quality based only on the model simulation results. This reviewer full agree that the presented observational data set in this study are unique and very useful to understating the level of air pollution in the study area. However, in this revised manuscript, there are several important issues on model simulation and scientific discussion. Therefore, this revised manuscript cannot be accepted in its current form. Before publishing in ACP, several points should be clarified.

We would like to thank the reviewer for his/her constructive comments and suggestions. It seems to us that the reviewer provided suggestions based on the ACPD version (date: 17th June, 2016) of the manuscript which makes it difficult to address all of the concerns. For example, based on the earlier reviewers' comments/suggestions, model based aerosol chemical composition has already been removed. However, we have tried our best to accommodate all of the suggestions to the possible extent. Please find the reviewer's comments in black and our replies in blue. The changes in the revised manuscript are colored in red.

Specific comments and suggestions are below:

L68, Fig 1: Information given in Figs 1, 2 and 5 are overlapped. This reviewer recommends to merge Fig 1 and Fig 5. That is, plot both monthly mean AOD and winds for separately in April, May and June. Those figures will give more direct insight on aerosol distribution and regional-scale circulation during the intensive measurement period. Fig 2 is not necessary in main body text, so please move it to the supplement.

As suggested by the reviewer, Figure 1 and Figure 5 have been merged which is the new Figure 1 in the revised version of the manuscript. Likewise, Figure 2 has been moved to the supplementary information section as Figure S1.

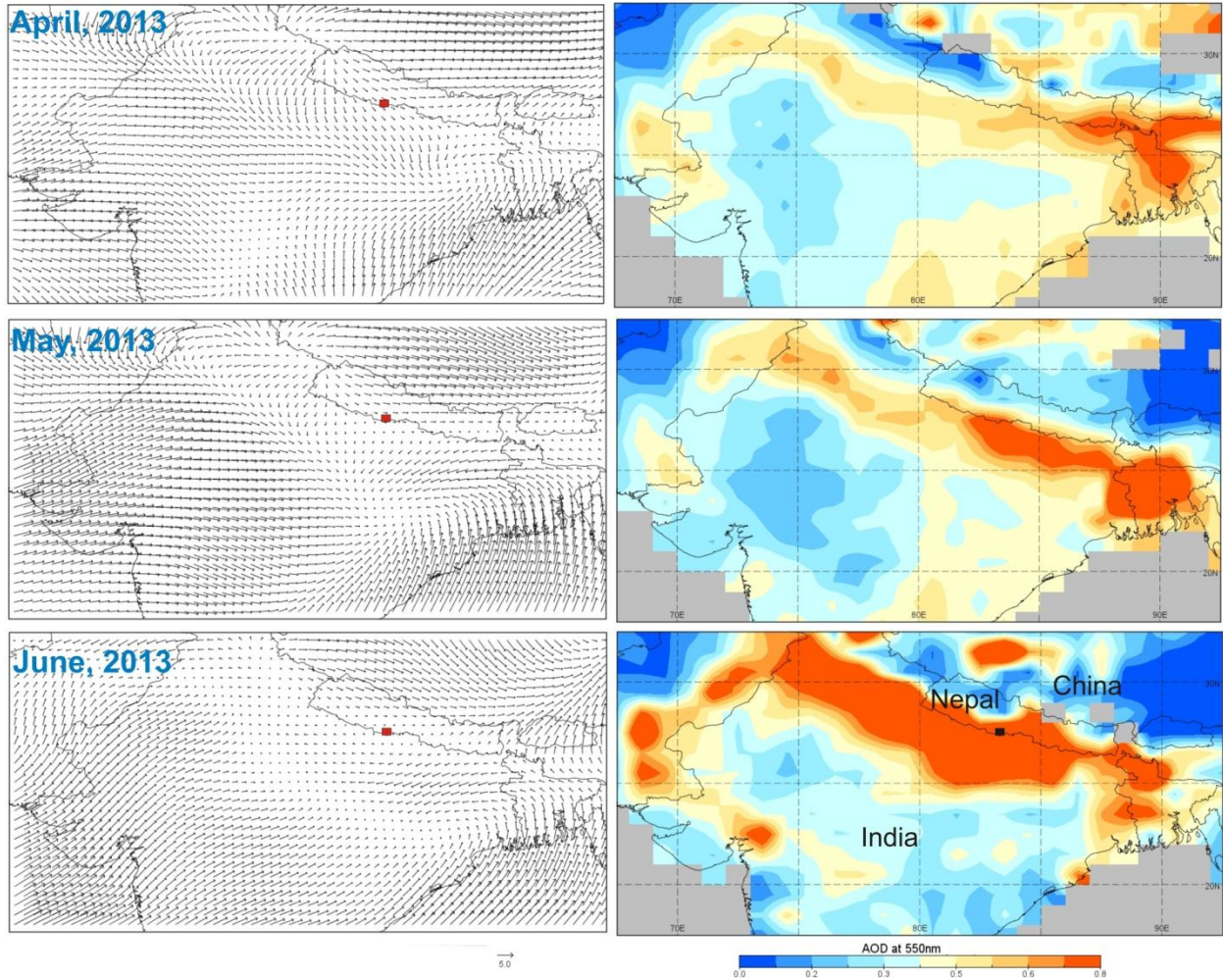


Figure 1. Monthly synoptic wind (at 1000 hPa) for April, May and June 2013, based on NCEP/NCAR reanalysis data where the orientations of arrows refer to wind direction and the length of arrows represents the magnitude of wind (m/s). Red square box in the figure (left) represents the location of Lumbini. Figures on the right column represent monthly aerosol optical depth acquired with the MODIS instrument aboard TERRA satellite. High aerosol loading can be seen over the entire Indo-Gangetic Plains (IGP). Light gray color used in the figure represents the absence of data.

L68, Fig 1: Which version of MODIS TERRA data have used? Why the authors are not used MODIS Aqua data?

Version 6 (Level 3) of the MODIS TERRA AOD data has been used in this study. We looked at both Aqua and Terra images, which are as follows. They are not significantly different. The difference between the AOD values from two satellites could be due to the true diurnal signal or the retrieval error (Wang et al., 2010).

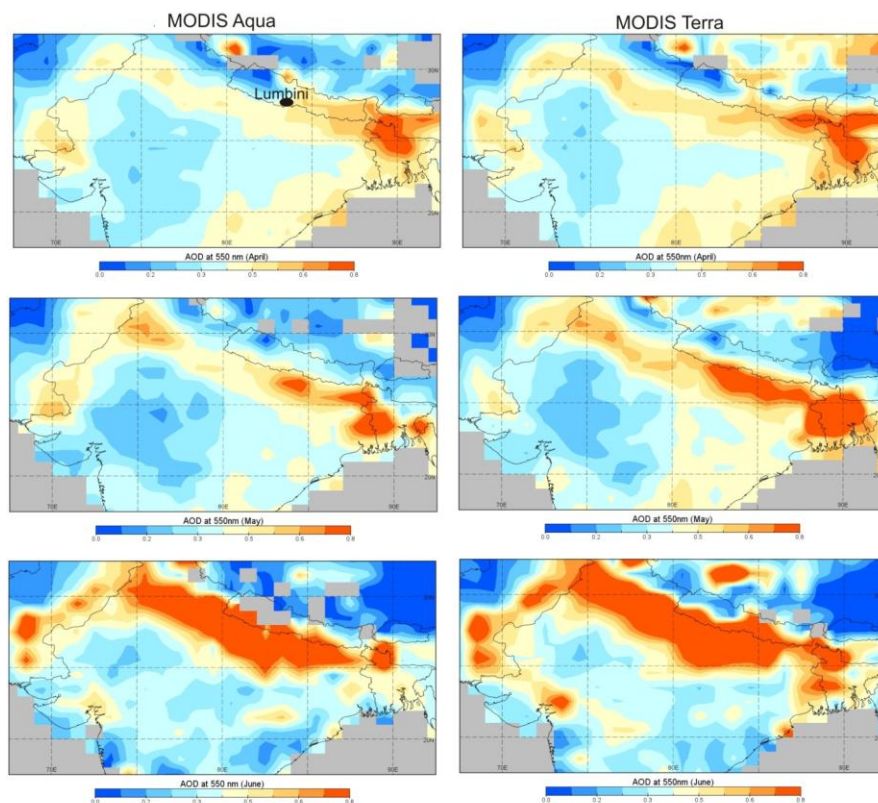


Figure: Monthly average MODIS Aqua and Terra AOD over the South Asian region during April-June, 2013. The black dot indicates the location of Lumbini.

Reference:

Wang, L., Wang, Y., Xin, J., Li, Z., & Wang, X. (2010). Assessment and comparison of three years of Terra and Aqua MODIS Aerosol Optical Depth Retrieval (C005) in Chinese terrestrial regions. *Atmospheric Research*, 97(1), 229-240.

L54-139: This reviewer recommends to reduce the length of INTRODUCTION section with deleting sentences are not closely related the topic of this paper. For example, the authors emphasize many times in the paper that Lumbini is a UNESCO world heritage. This is interested to the authors, but not to all readers. So please minimize the statements on this.

&

L 99 ~ : As the authors mentioned, sulfuric acid is more critically important in historical heritages. Please more carefully and clearly explain why the air pollutants presented in this study is important should added in the INTRODUCTION.

Agreed. The unwanted length of the Introduction section has been reduced along with the minimal use of information on UNESCO world heritage in this section. The deleted sentences are indicated with the strikethrough. In addition, the significance of the monitored species has been mentioned in the Introduction.

L128: remove “Aerosol optical depth – not discussed on the present study”. This is not necessary here.

Agreed and has been removed.

L 165: Table 1 - The sampling period should be more clearly clarified. As shown in Fig. 6, all instruments had not properly operated during the study period.

Done. All instruments ran successfully for the entire duration of the campaign except PM instrument. The following text has been inserted in Section 3.2.1.

“The gap in the figure (for PM time series) is due to the power interruption to the instrument.”

L169: What’s the uncertainty of PM concentration measured with GRIMM EDM164? Especially the quantitative uncertainty of EDM164 for such a high PM concentration level should be discussed, because PM concentration in here is estimated from light scattering measurements.

PM concentrations have been observed highly variable as evident in the standard deviations. For example, variability in PM₁, PM_{2.5} and PM₁₀ concentration for the month of April is 67.8 %, 60.2 % and 61.8 % respectively from their mean. Similar values were obtained during the month of

May whereas lower values were obtained for the month of June (PM_1 : 43.6%, $PM_{2.5}$: 45.3 % and PM_{10} : 54.1 %). The instrument deployed for PM concentration measurement (GRIMM EDM164) is able to measure the particles mass concentration in the range of 0.1-6000 $\mu\text{g}/\text{m}^3$ with the size ranging between 0.25-32 μm with an accuracy of $\pm 5\%$ over the entire measurement range (GRIMM EDM-164 manual; available at : http://wiki.grimm-aerosol.de/images/3/31/GRIMM_EDM_164_datasheet.pdf). Given the high range of the instrument for PM concentration monitoring as compared to that found on our study site, we strongly believe that the data provided by the instrument is highly trustworthy.

Figures 3 & 6 : There is large differences between observations and model simulations. First, more specific explanation and discussion on why the model results were not well agreed with the observations must be addressed. Why the WRF-STEM simulation cannot well simulate the precipitation events and why there is big difference in RH, WD and WS. Why BC is too underestimated compare to the aethalometer data? This should be made for all parameters. This is very important to convincing the results given in Section 3.3 and Section 3.4, as the authors mentioned in L261-262.

The revised version of the paper (submitted on 10th February, 2017) has already addressed this issue. For your information, various sentences on observation and model comparison (on the concentration part) were already removed as suggested by the previous reviewers. In addition, we have applied some general statistics to understand the relationship between observed and modeled species. Please see our response to another reviewer.

Since this is not only modeling based study, it is beyond the scope of the current paper to do sensitivity analysis with different physics scheme or initial and boundary conditions to improve the meteorological prediction. Besides, comparing one station data point with model grid representing 25x25 km is always difficult. We present the comparison results of model to observation to indicate model performance over Lumbini region, not as model validation. We do not have the local emissions inventory and thus we are using the global EDGAR emission in our model. There are plenty of published papers that have used global EDGAR emissions for regional modeling analysis.

Figure 3: WD should NOT be plotted with solid line, because, for example, WD at 355 and 5 degree is almost the same direction. So make a plot with dots.

Agree. The line graph for the WD has been replaced by the dots.

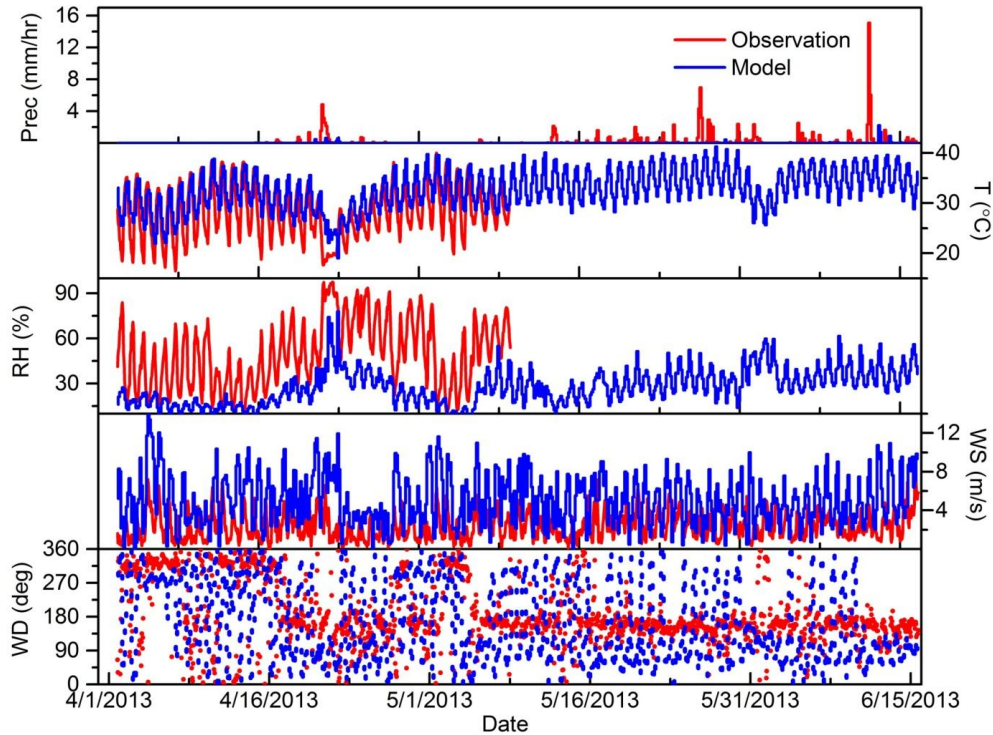


Figure 2. Time series of hourly average observed (red) and model estimated (blue) meteorological parameters at Lumbini, Nepal for the entire measurement period during 1 April to 15 June 2013

L242-243: It is hard to agree to this argument. As shown in Fig. 3, there is large difference between modeled and observed wind speed.

This sentence was already revised during the first revision. We would like to reiterate that the model was able to capture the pattern but not the magnitude; the magnitude by the model is overestimated as compared to the observation which is a common feature of WRF model. Past studies have also proved that the WRF model generally overestimates the WS (Borge et al., 2008; Mohan & Bhati, 2011; Hu et al., 2013; Gunwani & Mohan, 2017).

References

- Borge, R., Alexandrov, V., Del Vas, J. J., Lumbreras, J., & Rodríguez, E. (2008). A comprehensive sensitivity analysis of the WRF model for air quality applications over the Iberian Peninsula. *Atmospheric Environment*, 42(37), 8560-8574.
- Mohan, M., & Bhati, S. (2011). Analysis of WRF model performance over subtropical region of Delhi, India. *Advances in Meteorology*, 2011.
- Hu, X. M., Klein, P. M., & Xue, M. (2013). Evaluation of the updated YSU planetary boundary layer scheme within WRF for wind resource and air quality assessments. *Journal of Geophysical Research: Atmospheres*, 118(18).
- Gunwani, P., & Mohan, M. (2017). Sensitivity of WRF model estimates to various PBL parameterizations in different climatic zones over India. *Atmospheric Research*, 194, 43-65.

L258-259: This reviewer also cannot agree to this conclusive sentence. Apparently, the observed RH is two times higher than the modeled one. There is no evidence that RH by model is how well captured the regional variation. Is there a reference data to back this up?

RH values are highly underestimated by the model, however as previously mentioned as in the case of temperature (Section 3.1); the model does not show significant changes in RH during the measurement campaign when the observations stopped working.

L265- Figure 5: How about the winds at 850 hPa or 700 hPa pressure level?

New figures on the winds at 850 hPa have been plotted as follows. Please see the revised text for the discussion.

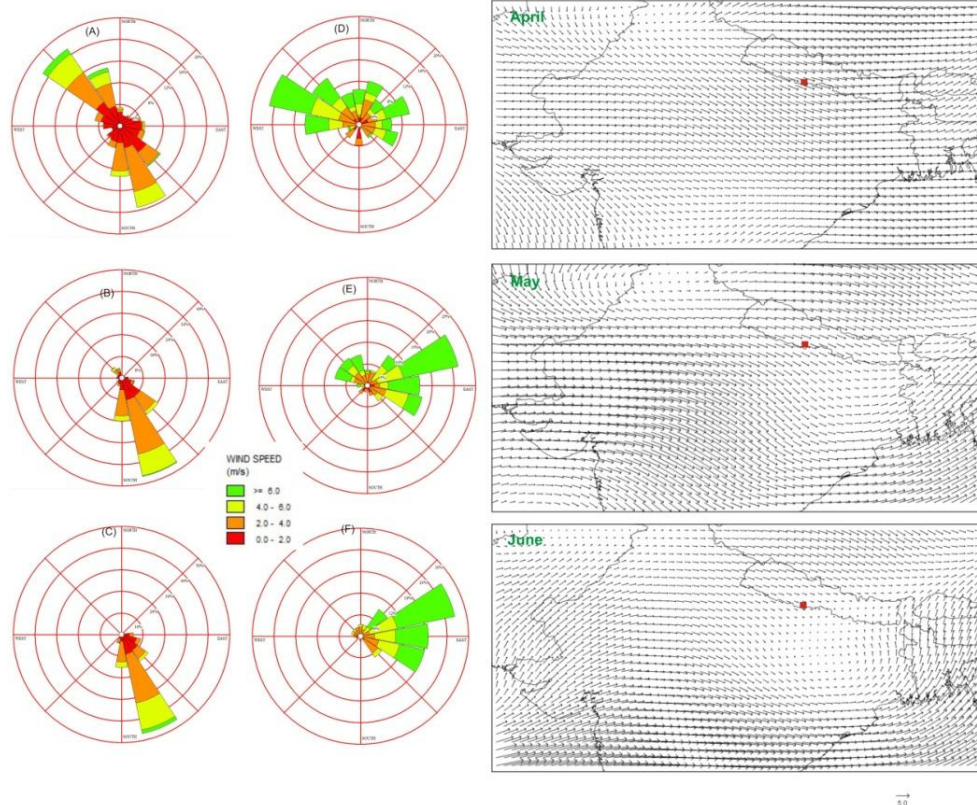


Figure S3: Wind rose of wind speed and wind direction obtained from the observation (A, B, C) and from the model (D, E, F) for the months of April, May and June 2013 respectively. The right panel shows the synoptic scale wind (850 hPa) during three months of the campaign.

L266-267: Here, what “calm winds” means? This discussion in Figure 6 is conflict the winds discussed in Figures 3 and 4. Please clarify.

“Calm winds” has been replaced by weak winds. The wind direction in Figure 3 (now Figure 2) has been replaced with the dot plot whereas Figure 4 deals with the monthly wind rose plot. However, no weather parameters have been plotted in Figure 6 as the reviewer has indicated. So, we are unable to address this comment.

Figure 6: As commented above, more explanations are needed why there is a large discrepancy between modeled and observed values. Without clarifying this, the results given in the next sections (sections 3.3.2. and 3.4) are not truly reliable.

As previous reviewers have also indicated this, the model output results and associated text have already been revised with unrelated text removed.

L384-385: This reviewer understands the PBL height observation was not available during the measurement period. However, the modeled PBL height has also large uncertainty and not believes it. The authors cited several previous works, but need to add some information on the PBL height, not general seasonal characteristics.

As suggested by the reviewer, we have added following sentences in the PBL description section:

The daily average PBL height obtained from the model is compared with published values (*Wan et al., 2017*) which indicate that the value is captured by our model during initial measurement period and overestimated in the months of mid May onwards. The monthly average diurnal variation also showed that the boundary layer height was maximum during 15:00 local time which coincides with the period of lowest concentration of the pollutants.

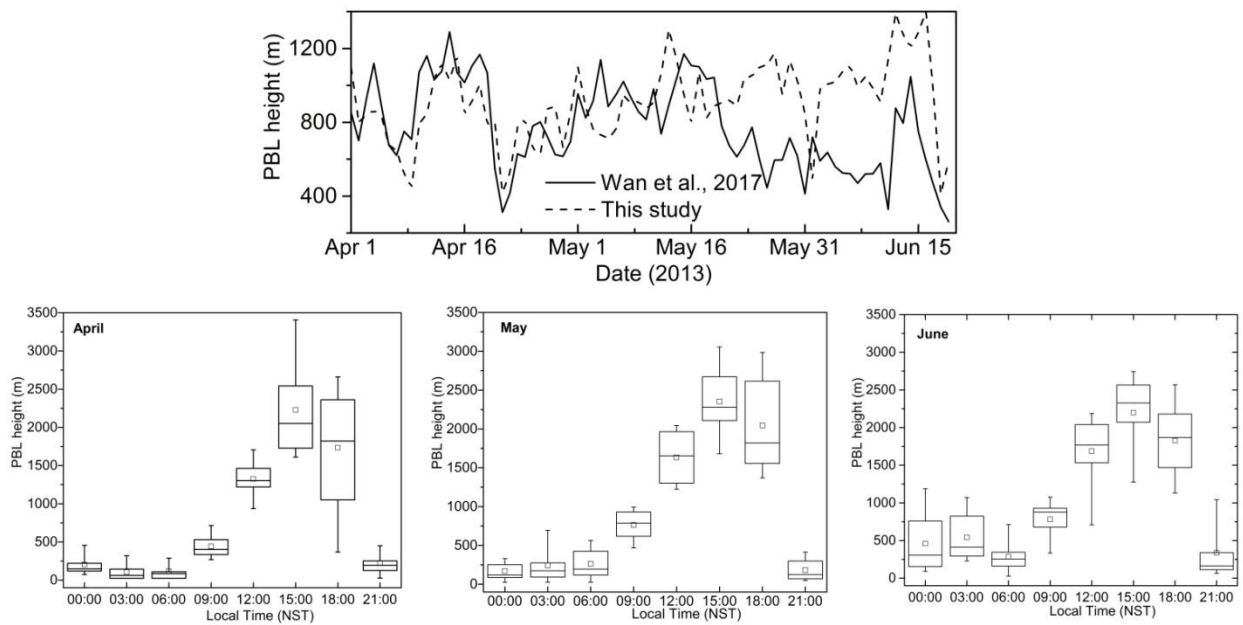


Figure 6. Daily time series of PBL height obtained from the model and reported values over Lumbini (obtained from Wan et al., 2017). The lower panel shows the monthly average diurnal variation of the PBL height. The square mark in each box represents the mean PBL height,

bottom and top of the box represents 25th and 75th percentile, top and bottom of the whisker represents 90th and 10th percentile respectively.

Reference

Wan, X., Kang, S., Li, Q., Rupakheti, D., Zhang, Q., Guo, J., . . . Cong, Z. (2017). Organic molecular tracers in the atmospheric aerosols from Lumbini, Nepal, in the northern Indo-Gangetic Plain: Influence of biomass burning. Atmos. Chem. Phys. Discuss., 2017, 1-40. doi:10.5194/acp-2016-1176 (Accepted for ACP).

L407-408: The authors mentioned ‘Global Monthly Fire Location Products’ were used. However, daily data were used in Figure 9. Please clarify this.

Thanks for pointing out the mistake. The daily data on forest fire were obtained from the FIRMS platform of NASA Earthdata. Correction has been done.

L416: Clearly present how much higher? This is very vague sentence.

We have revised the sentence as:

High AAE values (~ 1.6) during these two events are also an indication of presence of BC of biomass burning origin.

L421: Quality of Figure 10 is very bad. It’s hard to read.

We replaced it with high-resolution figure which is now Figure 8. The new figure is given below.

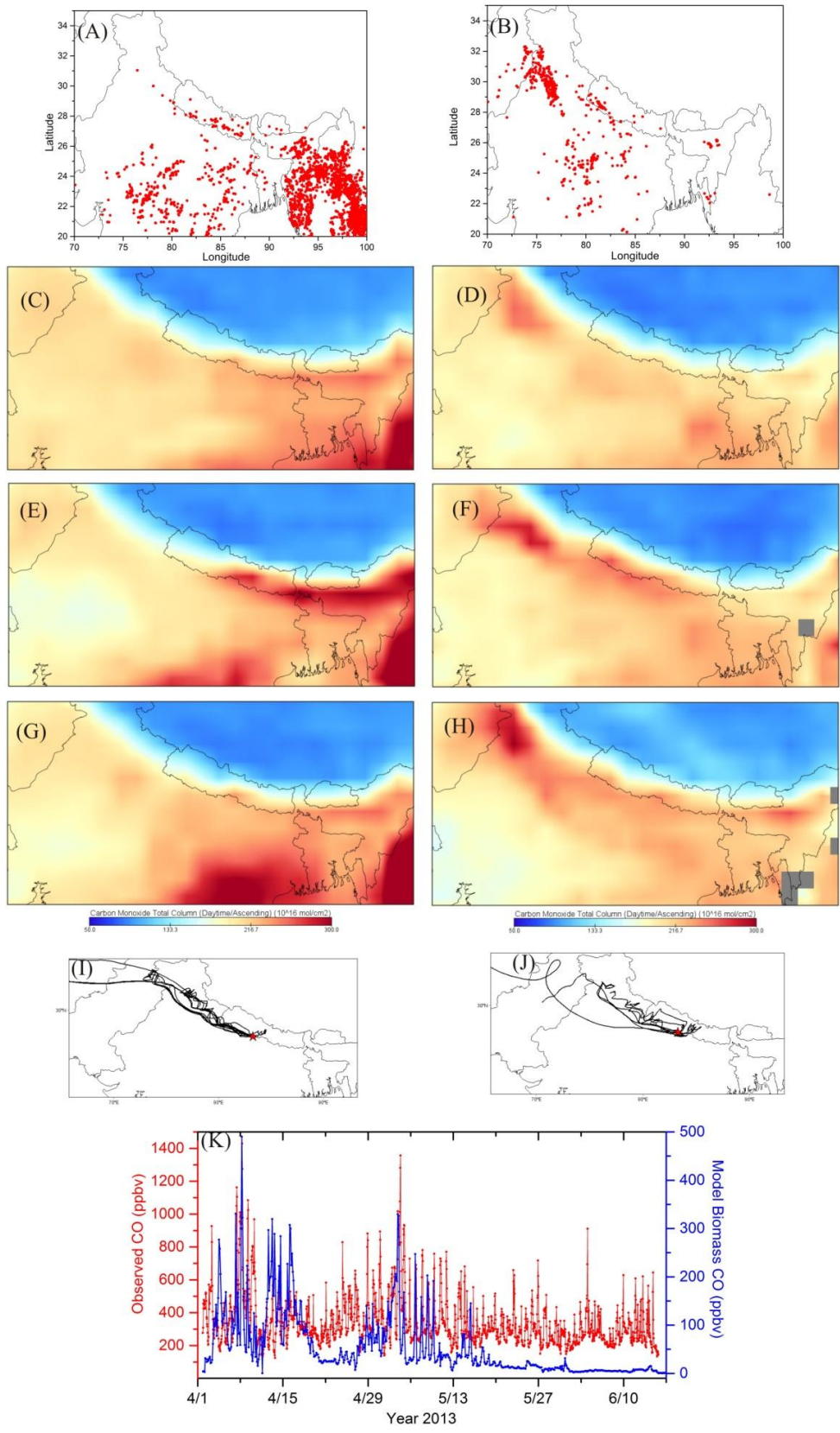


Figure 8. Active fire hotspots in the region acquired with the MODIS instrument on Aqua satellite during (A) Event-I (7-9 April) and (B) Event-II (3-4 May). CO emissions, acquired with AIRS satellite, in the region two days before (3-5 April), during (7-9 April) and two days after (10-12 April) Event-I are shown in panels (C), (E) and (G), respectively while panels (D), (F) and (H) show CO emissions two days before (1-2 May), during (3-4 May) and two days after (5-6 May) the Event-II. Panels (I) and (J) represent the 6-hr interval HYSPLIT back trajectories during Event I and II, respectively. Location of the Lumbini site is indicated by the red star in the panel (I and J). Observed CO versus Model open burning CO illustrating the contribution of forest fires during peak CO loading is shown in panel (K).

Figure 10: How the authors get the modelled biomass CO concentration? Generally the modelled biomass CO concentration is not capture the observed CO concentration. What is the major reason that the author gusse? This reviewer cannot agree to the sentence given in Li435-436.

STEM model can tag the CO emissions originating from biomass burning separately. Comparison of the model to observed CO is done by adding the biomass CO and anthropogenic CO together. This is a standard modeling technique employed by other air quality models as well. Since anthropogenic emissions do not change significantly in a weekly time scale and the temporal variability of the modeled biomass CO matches the temporal variability in the observation, it is inferred that the peak CO events are due to biomass burning. Meteorology could have played a role but we do not see a huge difference in modeled meteorology during the campaign period and observations are not available throughout the campaign.

Figure 10 (I) and (J): Instead of wind roses, regional-scale wind patterns will be more helpful to understand the transport in the interested region.

Thank you for pointing this. From the ground-based observation, we see the local winds coming from the south (for Event-I) whereas the HYSPLIT air mass and synoptic wind both showed that the air mass passed over the fire events in NW IGP. We have replaced the wind rose with the HYSPLIT back trajectories and corrected the text accordingly in section 3.3.1. In addition, the figures for regional-scale wind pattern (during these two events) have been provided in Figure S8 (supplementary materials).

L441-450 and Figure 11: The two ozone peaks were possible contributed by local pollution, induced by NO₂, but also by the transport from the fire plume. However, satellite NO₂ data shown in Figure 11 is not direct evidence of the effects of fires on high ozone concentration. Clarify this.

It is likely that the local pollution as well as regional pollution (transported from NW IGP region, as indicated by synoptic wind in Fig S8) contributed to the ozone peak. However, we are not able to quantify the individual contributions, even with the model simulation because ozone was not simulated in this experiment. These statements have been added to the text in Section 3.3.1.

L455 and Figure 12: It should be provided how the authors calculated the contributions from different countries? Can you provide PSCF results to back this up? In addition, have the authors estimated other pollutants (i.e., PM_{2.5} and PM₁₀) for their contribution like CO?

The source regions are identified using CO as a tracer as this is the standard techniques employed by other air quality models (Liu et al., 2003; Price et al., 2003; Pfister et al., 2005; Chen et al., 2009). CO emissions can be tagged according to the country of origin or any given area in the model and subsequently calculate the resulting concentration. The result shown in Figure 10 (current revised version) is done using this methodology. PSCF results are beyond the scope of the current manuscript. We haven't estimated the source regions for other pollutants like PM.

References

- Chen, D., Wang, Y., McElroy, M. B., He, K., Yantosca, R. M., & Sager, P. L. (2009). *Regional CO pollution and export in China simulated by the high-resolution nested-grid GEOS-Chem model. Atmospheric Chemistry and Physics, 9(11), 3825-3839.*
- Price, H. U., Jaffe, D. A., Doskey, P. V., McKendry, I., & Anderson, T. L. (2003). *Vertical profiles of O₃, aerosols, CO and NMHCs in the northeast Pacific during the TRACE-P and ACE-Asia experiments. Journal of Geophysical Research: Atmospheres, 108(D20).*
- Pfister, G., Hess, P. G., Emmons, L. K., Lamarque, J. F., Wiedinmyer, C., Edwards, D. P., ... & Sachse, G. W. (2005). *Quantifying CO emissions from the 2004 Alaskan wildfires using MOPITT CO data. Geophysical Research Letters, 32(11).*
- Liu, H., Jacob, D. J., Bey, I., Yantosca, R. M., Duncan, B. N., & Sachse, G. W. (2003). *Transport pathways for Asian pollution outflow over the Pacific: Interannual and seasonal variations. Journal of Geophysical Research: Atmospheres, 108(D20).*

Figure 14: The authors only showed wavelength dependency of normalized light-absorption coefficients for two time periods. First question is why the authors do not show all times? The authors can present with time (x-axis), wavelength (y-axis) and normalized light-absorption coefficient with different color. This figure will be more helpful to understand the difference of light-absorption coefficient in around 380 nm wavelength. Second, the difference at 380 nm in current Figure 14 is statistically significant? And how many data points were used? Last question for Figure 12 is that data during the fire periods discussed section 3.2 were included or excluded here?

The time period selected for Figure 14 (now Figure 11) refer to the periods when the BC concentration was highest and lowest as inferred from the diurnal variation of the BC (Figure 5). Our interest was to study the inclination of the curve during biomass burning dominated period (highest peak in the morning) and fossil fuel dominated period (during afternoon since there is the absence of cooking activities) in Lumbini. We chose those two periods of the day in this study. A new figure has been drawn (shown below) to understand the time series of the normalized light absorption which clearly indicates the highest values of the light absorption at the lowest wavelength. However, to our understanding, this figure possesses difficulties for comparison with reported normalized light absorption values (from literature) which leads us to retain the original figure. But we have included the normalized curve for both of the events which clearly indicated the inclination towards the biomass burning curve. The difference at 380 nm in Figure 11 is statistically insignificant at $p < 0.05$. The number of data points used for the cooking and non-cooking periods is 58 for each (excluding the data during two events). Figure 12 does not demonstrate the influence of forest fire, thus we are unable to provide our response to the later part of the query.

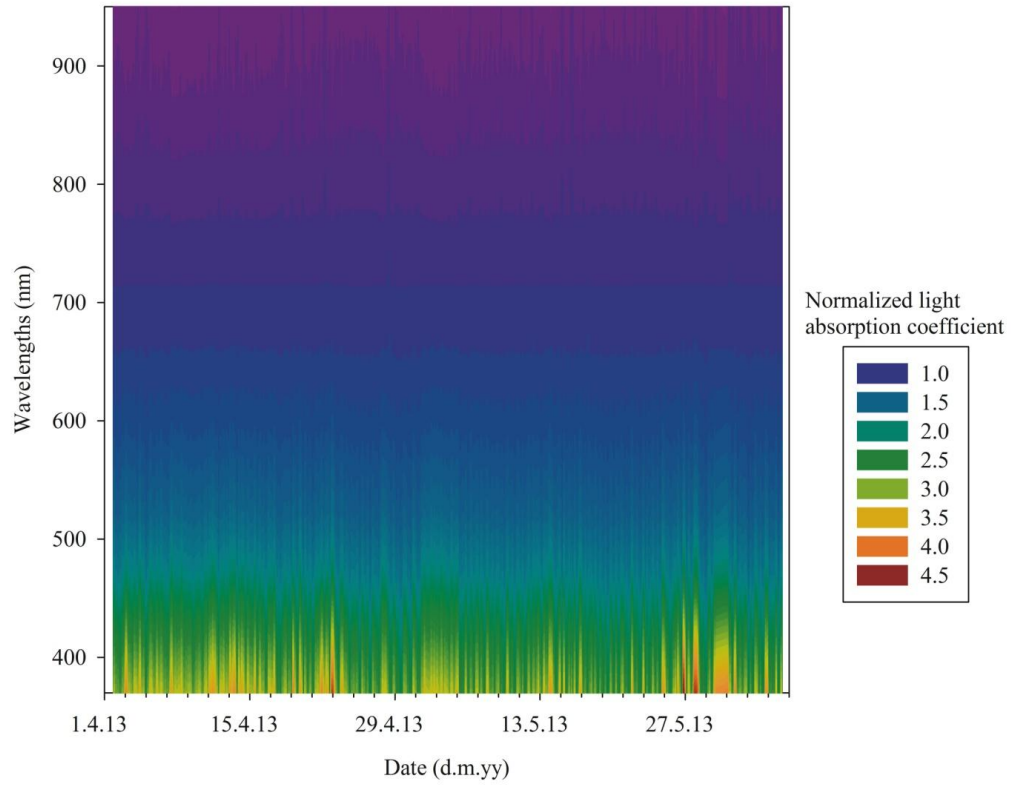


Figure: Time series of the normalized light absorption coefficient (normalized at 700nm) observed at Lumbini during the pre-monsoon of 2013.

Comments

Overall comment: The authors have improved the MS significantly, especially the monitoring data analysis and interpretation. The major uncertainty however still remains with the modeling part and it was, as pointed out by the authors, mainly due to the emission input data.

We would like to thank the reviewer for his/her comments/suggestions on our work. Please find the reviewer's comments in black and our replies in blue. The changes in the revised manuscript are colored in red.

Major comments:

It is not clear how authors extracted/projected the emission provided by EDGAR-HTAP_v2 for the simulation period and how the emissions were segregated temporally (hourly, daily etc.) for the simulation.

Emissions provided by the EDGAR-HTAP_v2 were re-gridded using four point interpolation technique available in the STEM model emissions preprocessor. The STEM model has been used extensively to study air pollution in Asia. The model has parameterized diurnal emission profile built in the emission preprocessor. Biomass emissions vary on a daily basis as per the burning event detected by FINN model while other anthropogenic emissions are constant over the year without seasonality.

One of the reasons of the discrepancy between the modeled and monitored levels is the point-based monitoring as compared to model produced grid average values. However, the model significantly underestimated all species, especially PM. Even CO levels were not reasonably produced as shown in Figure 6, the two events were not reproduced that well (as stated in line 509) as the modeling results appear to be fluctuating continuously during the period.

Why modeled PM levels are not presented in Figure 6? It is suggested that authors include scatter plots to show the relationship between the monitoring and modeling results for each species in Figure 6. Due to the uncertainty in the model output, all the results and discussion based on the model results may be questionable, i.e. those discussed in Section 3.3.2 (line 524).

The PM composition and quantity discussion are removed in the current version of the manuscript based on the suggestions provided by the previous reviewers. To show improvement in emission inventory and model development, PM comparison statistics between model and observations are shown in Table 3.

Section 2.3: provide the reasons why this particular model was selected, i.e. if it performs better than other models for the region etc., and how the emission input data was prepared for the modeling period.

STEM model has been used extensively to study air pollution in Asia and other parts of the world since its creation in 1987. The model PI, Professor Gregory R. Carmichael has more than 25000 paper citations (Google Scholar Search) mostly based on STEM model studies. We believe that all models have strengths and weaknesses. The authors chose this model because of familiarity with this model.

Emissions provided by the EDGAR-HTAP_v2 were projected using the four point interpolation technique available in the STEM model emissions preprocessor. The model has parameterized diurnal emission profile built in the emission preprocessor. Biomass emissions can vary on a daily basis as per the burning event detected by FINN model while other anthropogenic emissions are constant over the year without seasonality.

Section 3.1: WRF overestimated temperature and wind speed, underestimated precipitation and RH. Common statistical measures should be used to assess the model performance. For wind direction, because of the circular scale of the measurements (near 0 and near 360 degrees are almost the same) the interpretation of the time series should be made with caution or should be avoided. The comparison should be made for different wind sectors or simply by comparing the modelled windroses with the observed windroses to be presented along in Figure 4.

Agree. Based on the suggestion of the reviewer, we calculated correlation, Root Mean Square Error (RMSE) and Mean Absolute Difference (MAD) for the observed and modeled meteorological parameters. The correlation (r) for wind direction, wind speed, temperature and relative humidity were found to be 0.18, 0.22, 0.87 and 0.71 (all values at $P < 0.001$) respectively.

Similarly, Root Mean Square Error (RMSE) and Mean Absolute Difference (MAD) were also calculated for the meteorological parameters. RMSE (MAD) values were found as 121.16 (105.67), 3.55 (3.10), 31.66 (27.24), 3.94 (3.28) for wind direction, wind speed, relative humidity and temperature respectively. The values obtained in our study are comparable with those from Delhi during summer as reported in Mohan & Bhati (2011) using the WRF model. Considering the circular scale of the wind direction measurement, we have replaced the line plot previously used for the time series of the wind speed by the dots. This suggestion was provided by another reviewer as well. Now, based on the suggestion by this reviewer, we have plotted the wind rose diagram for the model based values and presented along with the measurement based values as shown in the Figure S3 below. However, please note that comparing wind direction from a point source measurement to a model grid is always difficult. Besides, comparing surface wind direction is more challenging than at higher altitudes where more synoptic winds prevail. In the absence of vertical wind direction observations, we show the surface wind comparison just to indicate model performance, not as model validation. In addition, we also show NCEP/NCAR reanalysis plots in the figure to illustrate the difficulty in comparing wind direction for air pollution transport.

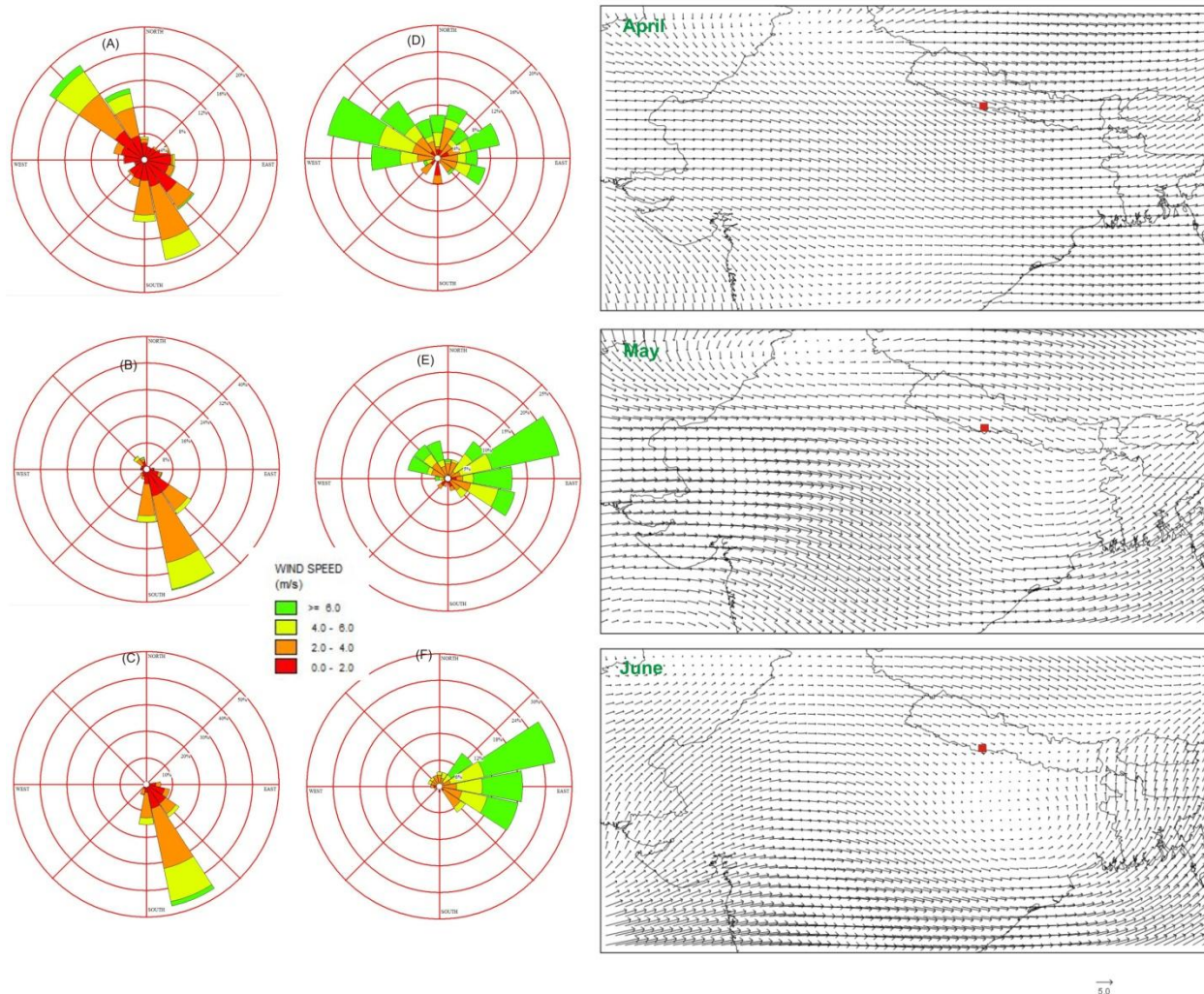


Figure S3: Wind rose of wind speed and wind direction obtained from the observation (A, B, C) and from the model (D, E, F) for the months of April, May and June 2013 respectively. The right panel shows the synoptic scale wind (850 hPa) during three months of the campaign.

Reference

Mohan, M., & Bhati, S. (2011). *Analysis of WRF model performance over subtropical region of Delhi, India. Advances in Meteorology, 2011.*

Suggestion: Since the purpose of using WRF-STEM model was “...to understand pollution source region as well as the contribution of open biomass burning to air quality in Lumbini...” as stated in lines 126-127, it is suggested that authors can use alternative ways of the data analysis

to achieve the same aims. For example, analysis of wind field (such as Figure 5) or HYSPLIT trajectories and source locations (hotspots, urban etc.) to show the potential of regional transport of the biomass smoke to the site.

Thank you for the suggestions. Another reviewer has suggested to move the synoptic scale wind to Figure 1 (along with the AOD) which we have agreed and revised the Figure 1 (please see our response to another reviewer). We have included the HYSPLIT (in Figure 8) to understand the possible source region for pollutants during two events. However, we wish to note that using back trajectories to identify source regions are also uncertain as identified by Jaffee et al. (1999).

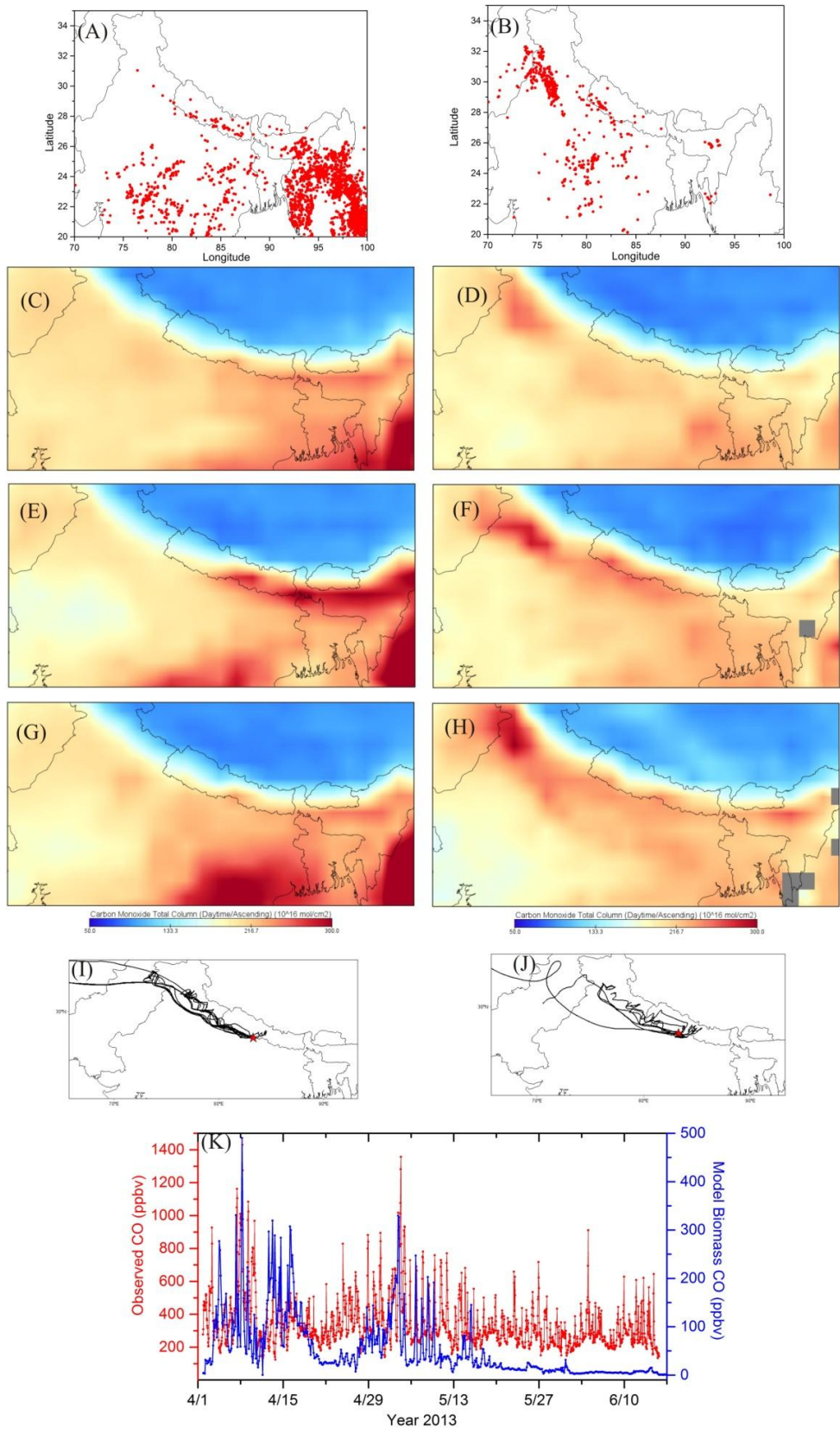


Figure 8. Active fire hotspots in the region acquired with the MODIS instrument on Aqua satellite during (A) Event-I (7-9 April) and (B) Event-II (3-4 May). CO emissions, acquired with AIRS satellite, in the region two days before (3-5 April), during (7-9 April) and two days after (10-12 April) Event-I are shown in panels (C), (E) and (G), respectively while panels (D), (F) and (H) show CO emissions two days before (1-2 May), during (3-4 May) and two days after (5-6 May) the Event-II. Panels (I) and (J) represent the 6-hr interval HYSPLIT back trajectories during Event I and II, respectively. Location of the Lumbini site is indicated by the red star in the panel (I and J). Observed CO versus Model open burning CO illustrating the contribution of forest fires during peak CO loading is shown in panel (K).

Reference

Jaffe, D., Anderson, T., Covert, D., Kotchenruther, R., Trost, B., Danielson, J., ... & Harris, J. (1999). Transport of Asian air pollution to North America. Geophysical Research Letters, 26(6), 711-714.

Minor comments:

Line 180: remove word “dust” because not only dust particles but all the particles

Done.

Line 387: the air pollution levels may not be the right/only criteria to classify an area into semiurban or rural etc. Please rephrase.

Done. The new sentence now reads as:

In addition, average BC and CO concentrations in Lumbini were found falling in between concentrations observed at rural sites (up to 6 times higher) and cities in the region (see Table 2), indicating that Lumbini, in a way, can still be considered as semi-urban location.

Line 449: too long a sentence. Please improve the written language.

Done. We have rephrased the sentence as:

Increase in CO concentrations in the evening hours might be due to transport of CO from source regions upwind of Lumbini which along with the local emissions get trapped under reduced Planetary Boundary Layer (PBL) heights.

Line 617: the content above shows important influence from open burning but the discussion in this section seems to be biased toward residential cooking.

The main aim of this section is to understand the influence of biomass burning on the air quality in Lumbini. Main source of biomass burning in the study area is residential cooking (as shown in Figure 11 and 12 in the current revised version). Due to this fact, we believe that the explanation represents the biomass burning which in a way stands for the residential cooking.

1 **Pre-monsoon air quality over Lumbini, a world heritage site**
2 **along the Himalayan foothills**

3 Dipesh Rupakheti^{1,2*}, Bhupesh Adhikary³, Puppala S. Praveen³, Maheswar Rupakheti^{4,5},
4 Shichang Kang^{6,7*}, Khadak S. Mahata⁴, Manish Naja⁸, Qianggong Zhang^{1,7}, Arnico K. Panday³,
5 Mark G. Lawrence⁴

6 ¹Key Laboratory of Tibetan Environment Changes and Land Surface Processes, Institute of
7 Tibetan Plateau Research, Chinese Academy of Sciences, Beijing 100101, China

8 ²University of Chinese Academy of Sciences, Beijing 100049, China

9 ³International Centre for Integrated Mountain Development (ICIMOD), Kathmandu, Nepal

10 ⁴Institute for Advanced Sustainability Studies (IASS), Potsdam 14467, Germany

11 ⁵Himalayan Sustainability Institute (HIMSI), Kathmandu, Nepal

12 ⁶State Key Laboratory of Cryospheric Science, Cold and Arid Regions Environmental and
13 Engineering Research Institute (CAREERI), Lanzhou 730000, China

14 ⁷Center for Excellence in Tibetan Plateau Earth Sciences, Chinese Academy of Sciences, Beijing
15 100085, China

16 ⁸Aryabhata Research Institute of Observational Sciences (ARIES), Nainital, India

17

18 **Correspondence to:*

19 D. Rupakheti (dipesh.rupakheti@itpcas.ac.cn), S.C. Kang (shichang.kang@lzb.ac.cn)

20

21 Abstract

22 Lumbini, in southern Nepal, is a UNESCO world heritage site of universal value as the
23 birthplace of Buddha. Poor air quality in Lumbini and surrounding regions is a great concern for
24 public health as well as for preservation, protection and promotion of Buddhist heritage and
25 culture. We present here results from measurements of ambient concentrations of key air
26 pollutants (PM, BC, CO, O₃) in Lumbini, first of its kind for Lumbini, conducted during an
27 intensive measurement period of three months (April-June 2013) in the pre-monsoon season. The
28 measurements were carried out as a part of the international air pollution measurement
29 campaign; SusKat-ABC (Sustainable Atmosphere for the Kathmandu Valley - Atmospheric
30 Brown Clouds). The main objective of this work was to understand and document the level of air
31 pollution, diurnal characteristics and the influence of open biomass burning on air quality in
32 Lumbini. The hourly average concentrations during the entire measurement campaign ranged as
33 follows: BC: 0.3 - 30.0 $\mu\text{g m}^{-3}$, PM₁: 3.6-197.6 $\mu\text{g m}^{-3}$, PM_{2.5}: 6.1 - 272.2 $\mu\text{g m}^{-3}$, PM₁₀: 10.5 -
34 604.0 $\mu\text{g m}^{-3}$, O₃: 1.0 - 118.1 ppbv, and CO: 125.0 - 1430.0 ppbv. These levels are comparable to
35 other very heavily polluted sites in South Asia. Higher fraction of coarse mode PM was found as
36 compared to other nearby sites in the IGP region. $\Delta\text{BC}/\Delta\text{CO}$ ratio obtained in Lumbini indicated
37 considerable contributions of emissions from both domestic and transportation sectors. The 24-h
38 average PM_{2.5} and PM₁₀ concentrations exceeded the WHO guideline very frequently (94% and
39 85% of the sampled period, respectively), which implies significant health risks for the residents
40 and visitors in the region. These air pollutants exhibited clear diurnal cycles with high values in
41 the morning and evening. During the study period, the worst air pollution episodes were mainly
42 due to agro-residue burning and regional forest fires combined with meteorological conditions
43 conducive of pollution transport to Lumbini. Fossil fuel combustion also contributed
44 significantly, accounting for more than half of the ambient BC concentration according to
45 aerosol spectral light absorption coefficients obtained in Lumbini. WRF-STEM, a regional
46 chemical transport model, was used to simulate the meteorology and the concentrations of
47 pollutants to understand the pollutant transport pathways. The model ~~was able to reproduce the~~
48 ~~temporal variation in the pollutant concentrations well; however,~~ estimated values were ~ 1.5 to
49 5 times lower than the observed concentrations for CO and PM₁₀ respectively. Model simulated
50 regionally tagged CO tracers showed that the majority of CO came from the upwind region of

51 Ganges Valley. Model needs significant improvement in simulating aerosols in the region.
52 Given the high pollution level, there is a clear and urgent need for setting up a network of long-
53 term air quality monitoring stations in the greater Lumbini region.

54 1. Introduction

55 The Indo-Gangetic plain (IGP) stretches over 2000 km encompassing a vast area of land in
56 northern South Asia: the eastern parts of Pakistan, most of northern and eastern India, southern
57 part of Nepal, and almost all of Bangladesh. The Himalayan mountains and their foothills stretch
58 along the northern edge of IGP. The IGP region is among the most fertile and most intensely
59 farmed region of the world. It is a heavily populated region with about 900 million residents or
60 12% of the world's population. Four megacities - Lahore, Delhi, Kolkata, and Dhaka are located
61 in the IGP region, with dozens more cities with populations exceeding one million. The region
62 has witnessed impressive economic growth in recent decades but unfortunately it has also
63 become one of the most polluted, and an air pollution 'hot spot' of local, regional and global
64 concern (Ramanathan et al., 2007). Main factors contributing to air pollution in the IGP and
65 surrounding regions include emissions from vehicles, thermal power plants, industries, biomass
66 and fossil fuel used in cooking and heating activities, agricultural activities, crop residue burning
67 and forest fires. Air pollution gets transported long distances away from emission sources and
68 across national borders. As a result, the IGP and adjacent regions get shrouded with a dramatic
69 annual buildup of regional scale plumes of air pollutants, known as Atmospheric Brown Clouds
70 (ABC), during the long and dry winter and pre-monsoon seasons each year (Ramanathan and
71 Carmichael, 2008). **Figure 1 shows monthly synoptic wind and mean aerosol optical depth**
72 **(AOD) during April-June, 2013 over South Asia. ~~acquired from the MODIS instrument onboard~~
73 ~~TERRA satellite over South Asia for a period of December 2012-June 2013.~~ Very high aerosol
74 optical depth along the entire stretch of IGP reflects severity of air pollution over large areas in
75 the region.**

76 Poor air quality continues to pose significant threat to human health in the region. In a new study
77 of global burden of disease released recently, Forouzanfar et al. (2015) estimated that in 2013
78 around 1.7 million people died prematurely in Pakistan, India, Nepal, and Bangladesh as a result
79 of air pollution exposure, nearly 30% of global total premature deaths due to air pollution. Air

80 pollution also affects precipitation (e.g. South Asian monsoon), agricultural productivity,
81 ecosystems, tourism, climate, and broadly socio-economic and national development goals of the
82 countries in the region (Burney and Ramanathan, 2014;Shindell, 2011;Ramanathan and
83 Carmichael, 2008). It has also been linked to intensification of cold wave and winter fog in the
84 IGP region over recent decades (Lawrence and Lelieveld, 2010 and references therein;Safai et
85 al., 2009;Ganguly et al., 2006). Besides high levels of aerosol loading as shown in Fig. 1, Indo-
86 Gangetic plains also have very high levels of ground level ozone or tropospheric ozone (O₃)
87 (e.g., Ramanathan and Carmichael (2008))—~~It~~ **which** is a toxic pollutant to plant and human
88 health, and a major greenhouse gas (IPCC, 2013;Shindell, 2011;Mohnen et al., 1993). South
89 Asia, in particular IGP region, has been projected to be the most ozone polluted region in world
90 by 2030 (Stevenson et al., 2006). Majority of crop loss in different parts of the world results from
91 effects of ozone on crop health and productivity (Shindell, 2011). Burney and Ramanathan
92 (2014) also reported a significant loss in wheat and rice yields in India from 1980 to 2010 due to
93 direct effects of black carbon (BC) and ozone (O₃). BC and O₃ are two key short-lived climate
94 pollutants (SLCP). **Similarly, species like fine particles and carbon monoxide (CO) are potent to**
95 **health damages by posing impacts upon the respiratory and cardiovascular system and even also**
96 **to the climate system (Singh et al., 2017 and references therein).** Because of the IGP's close
97 proximity to the Himalaya-Tibetan plateau region, this once relatively clean region, is now
98 subjected to increasing air pollution transported from regions such as the IGP, which can exert
99 additional risks to sensitive ecosystems in the mountain region (e.g., (Lüthi et al., 2015;Marinoni
100 et al., 2013;Duchi et al., 2011). **However,** air pollution transport pathways to Himalayas are still
101 not yet fully understood.

102 Monuments and buildings made with stones are vulnerable to air pollution damage
103 (Brimblecombe, 2003;Gauri and Holdren, 1981). Sulfur dioxide, which forms sulfuric acid upon
104 reaction with water, is the most harmful substance for the monuments as it can corrode and
105 damage them (Baedecker et al., 1992;Gauri and Holdren, 1981). ~~Indo-Gangetic plains are rich in~~
106 ~~archeological, cultural and historical sites and monuments and many of them are inscribed as~~
107 ~~UNESCO World Heritage Site. For example, among many other such sites in IGP are the~~
108 ~~Archaeological Ruins at Moenjodaro (Pakistan), Taj Mahal in Agra and Mahabodhi Temple~~
109 ~~Complex in Bodh Gaya (India), Lumbini (Nepal), and ruins of the Buddhist Vihara at Paharpur~~

110 ~~(Bangladesh) (World Heritage List; UNESCO, website: <http://whc.unesco.org/en/list>).~~ The Taj
111 ~~Mahal is one of the seven wonders of the modern world and India's greatest landmark. At the~~
112 ~~end of the last century, the government of India realized the growing problem of air pollution~~
113 ~~damage to Taj Mahal and started a program to save the monument.~~ A recent study has reported
114 that deposition of light absorbing aerosol particles (black carbon, brown carbon) and dust is
115 responsible for the discoloration **of Taj Mahal, a world famous monument in India** (Bergin et al.,
116 2015). Lumbini, located near the northern edge of the central Ingo-Gangetic plain, is famous as
117 the birthplace of the Lord Buddha ~~.Lumbini is~~ and thus a UNESCO world heritage site of
118 outstanding universal value to humanity. ~~,inscribed in the UNESCO list since 1997. The site,~~
119 ~~with valuable archaeological remains of the Buddhist Viharas (monasteries) and Stupas~~
120 ~~(memorial shrines), as well as modern temples and monasteries, is a center of attraction and~~
121 ~~visited by hundreds of thousands of pilgrims, scientists, scholars, yogis, and tourists every year.~~
122 **Since the study area is renowned due to its historical and archaeological significance, Lumbini is**
123 **getting the worldwide attention also for poor air quality in the region.** There was no regular air
124 quality monitoring in Lumbini at the time of our measurement campaign.

125 Through this study, we want to understand the level of air pollution, its diurnal characteristic,
126 and the influence of open biomass burning on air quality in Lumbini. We carried out continuous
127 measurements of ambient concentrations of key air pollutants (particulate matter, black carbon,
128 carbon monoxide, ozone) and meteorological parameters during an intensive measurement
129 period of three months (April-June) in the year 2013. These are the first reported pollutant
130 measurements for Lumbini. A regional chemical transport model called Sulfur Transport and
131 dEposition Model (STEM) was used to simulate the variations of meteorological parameters and
132 air pollutants during the observation period ~~to understand pollution source region as well as the~~
133 ~~contribution of open biomass burning to air quality in Lumbini~~ **to examine the extent to which a**
134 **state-of-the-art, widely-used air quality model is able to simulate the data, as an indication for**
135 **where there are still gaps in our knowledge and what further measurements and emissions dataset**
136 **developments are needed.** Model simulated regionally tagged CO tracers were used to identify
137 emission source regions impacting pollutant concentration observed at Lumbini. Satellite data
138 has also been used to understand the high pollution events during the monitoring period. These
139 measurements were carried out as a part of the SusKat-ABC international air pollution

140 measurement campaign (*M. Rupakheti, manuscript in preparation for ACPD*) jointly led by the
141 International Centre for Integrated Mountain Development (ICIMOD), Kathmandu, Nepal and
142 Institute for Advanced Sustainability Studies (IASS), Potsdam, Germany.

143 2. Experimental set up

144 2.1 Sampling site

145 The Lumbini measurement site (27°29.387' N, 83°16.745' E, elevation: ~100 m above sea level)
146 is located at the premise of the Lumbini International Research Institute (LIRI), a Buddhist
147 library in Lumbini. Lumbini lies in the Nepal's southern lowland plain or *Terai* region, termed as
148 "bread basket of Nepal" due to the availability of very fertile land suitable for crop production,
149 which forms the northern edge of the Indo-Gangetic Plains (IGP). About 25 km north of Lumbini
150 the foothills begin while the main peaks of the Himalayas are 140 km to the north. The
151 remaining three sides are surrounded by flat plain land of Nepal and India. The site is only about
152 8 km from the Nepal-India border in the south. A three storied 10 m tall water tower was used as
153 the platform for the automatic weather station (AWS) whereas remaining instruments were
154 placed inside a room near the base of the tower. Figure S1 shows the location of Lumbini, the
155 Kenzo Tange Master Plan area of the Lumbini development project, and the sampling tower. An
156 uninterrupted power back up was set up in order to assure the regular power supply even during
157 hours with scheduled power cuts during the monitoring period. The nearby premises of the
158 monitoring site consist of the LIRI main office and staff quarters. Further away is a museum, a
159 local bus park for the visitors to Lumbini, the office of the Lumbini Development Trust,
160 monasteries, and thinly forested area with grassland within the master plan area. Outside of the
161 master plan area lie vast area of agricultural fields, village pockets, and several brick kilns and
162 cement industries. A local road (black topped), that cuts through the master plan area, lies about
163 200 m north of the sampling site and experiences intermittent passing of vehicles. According to
164 the Ministry of Culture, Tourism and Civil Aviation of Nepal over 130 thousand tourists
165 (excluding Nepalese and Indian citizens) visited the Lumbini area in 2014
166 (<http://tourism.gov.np/en>).

167 2.2 Monitoring Instruments

168 The summary of instruments deployed in Lumbini is presented in Table 1. All data were
169 collected in Nepal Standard Time (NST) which is GMT +05:45 hour. PM₁, PM_{2.5} and PM₁₀ mass
170 concentrations were monitored continuously with GRIMM EDM164 (GRIMM Aerosol Technik,
171 Germany) which uses the light scattering at 655 nm to derive mass concentrations. Similarly,
172 aerosol light absorptions at 7 wavelengths (370, 470, 520, 590, 660, 880, 950 nm) were
173 measured continuously with an Aethalometer (Model AE-42, Magee Scientific, USA), averaging
174 and reporting data every 5 min. It was operated at a flow rate of 5 l min⁻¹. No cut-off was applied
175 for inlet; hence the reported concentration of BC is total suspended BC particles. As described by
176 the manufacturer, ambient BC concentration is derived from light absorption at 880 nm using a
177 specific mass absorption cross section. To obtain BC concentration in Lumbini, we used a
178 specific mass absorption cross-section value of 8 m² g⁻¹ for the 880 nm channel. A similar value
179 has been previously used for BC measurement in the Indo-Gangetic plain (Praveen et al., 2012).
180 To remove the filter loading effect, we used correction method suggested by Schmid et al. (2006)
181 which was also used by Praveen et al. (2012) for BC measurements at a rural site in the Indo-
182 Gangetic plain. Surface ozone (O₃) concentration was measured continuously with an ozone
183 analyzer (Model 49i, Thermo Scientific, USA) which utilizes UV (254 nm wavelength)
184 photometric technology to measure ozone concentration in ambient air. CO analyzer (Model 48i,
185 Thermo Scientific, USA) was used to monitor ambient CO concentration which is based on the
186 principle that CO absorbs infrared radiation at the wavelength of 4.6 microns. The ambient air
187 was drawn through 6-micron pore size SAVILLEX 47 mm filter at the inlet in order to remove
188 the dust particles before sending air into the CO and O₃ analyzers using a Teflon tube. The filters
189 were replaced every 7-10 days depending on particle loading, based on manual inspection. CO
190 instrument was set to auto-zero at a regular interval of 6 hours. Local meteorological parameters
191 (temperature, relative humidity, wind speed, wind direction, precipitation, and global solar
192 radiation) were monitored with an automatic weather station (AWS) (Campbell Scientific,
193 Loughborough, UK), recording data every minute.

194 **2.3 Regional chemical transport model**

195 Aerosol and trace gas distributions were simulated using a regional chemical transport model.
196 Sulfur Transport and dEposition Model (STEM), a 3D eulerian model that has been used

197 extensively in the past to characterize air pollutants in South Asian region was used to **interpret**
198 **understand** observations at Lumbini (Kulkarni et al., 2015;Adhikary et al., 2007). The Weather
199 Research and Forecasting (WRF) model (Skamarock et al., 2008) version 3.5.1 was used to
200 generate the required meteorological variables necessary for simulating pollutant transport in
201 STEM. The model domain was centered at 24.94° N latitude and 82.55° E longitude covering a
202 region from 3.390° N to 43.308° N latitude and 34.880° E to 130.223° E longitude. The model
203 has 425×200 horizontal grid cells with grid resolution of 25×25 km and 41 vertical layers with
204 top of the model set at 50 mbar. The WRF model was run from November 1, 2012 to June 30,
205 2013. However, for this study, modeled data only from April to June 2013 have been used. The
206 WRF model was initialized with FNL data available from NCAR/UCAR site
207 (<http://rda.ucar.edu/datasets/ds083.2/>).

208 The tracer version of the STEM model provides mass concentration of sulfate, BC (hydrophilic
209 and hydrophobic), Organic carbon (OC), sea salt (fine and coarse mode), dust (fine PM_{2.5} and
210 PM₁₀), CO (biomass and anthropogenic) and region tagged CO tracers. STEM model domain
211 size, resolution and projection are those of the WRF model. Details about tracer version of the
212 STEM model is outlined elsewhere (Kulkarni et al., 2015;Adhikary et al., 2007). Anthropogenic
213 emission of various pollutants (CH₄, CO, SO₂, NO_x, NMVOC, NH₃, PM₁₀, PM_{2.5}, BC and OC)
214 used in this analysis were taken from the EDGAR-HTAP_v2
215 (http://edgar.jrc.ec.europa.eu/htap_v2/index.php?SECURE=123). Open biomass burning
216 emissions on a daily basis during the simulated period were taken from data obtained from the
217 FINN model (Wiedinmyer et al., 2011). Both these emissions were re-gridded to the STEM
218 model domain **using four point interpolation techniques available in the STEM model emissions**
219 **preprocessor**. As with the WRF model, the STEM model was run from November 2, 2012 to
220 June 30, 2013 however, data presented here are only during the intensive field campaign period.

221 3. Results and discussions

222 3.1 Meteorology

223 Hourly average time series of various meteorological parameters like precipitation in mm hr⁻¹
224 (Prec), temperature in °C (T), relative humidity in % (RH), wind speed in m s⁻¹ (WS) and

225 direction in degree (WD) during the monitoring period are shown in Figure 2. Meteorological
226 parameters were obtained with the sensors at the height of ~12 m from the ground. Meteorology
227 results from ~~simulations using~~ WRF model ~~simulations~~ have been used to ~~compare and fill the~~
228 ~~data gaps~~ indicate if any significantly different air mass was present during the measurement
229 campaign after the meteorological observations malfunctioned. Precipitation data was derived
230 from TRMM satellite (TRMM_3B42_007 at a horizontal resolution of 0.25°) from the Giovanni
231 platform (<http://giovanni.gsfc.nasa.gov/giovanni/>) as the rain gauge malfunctioned during the
232 sampling period. Precipitation data from TRMM (Figure 2) show that Lumbini was relatively dry
233 in the early portion of the measurement campaign while as the pre-monsoon edged closer to the
234 monsoon onset, the site did experience some rainfall events. This lowered aerosol loading in the
235 later half of the measurement campaign due to washout. Comparison of WRF model outputs
236 with TRMM data shows that the model under-predicts rainfall through out the campaign.

237 Average observed temperature for the sampling period until the sensor stopped working (on 8th
238 May, 2013, i.e., for 38 days of measurement) was 28.1°C (minimum: 16.5°C, maximum: 40°C).
239 Average temperature from the model, during same period, was 31°C with values ranging
240 between 19 - 40°C. As shown in Figure 2, the model captures the synoptic variability of
241 temperature and is mostly within the range of daily values. However, the model has a high bias
242 and does not capture well daily minimum temperature values. In addition, the model does not
243 show any large variation in temperature for the campaign period after the sensors stopped
244 working. This insight will be useful to interpret pollution data later on. For the same period (until
245 the sensor stopped working), the average (observed) RH was ~ 50% (ranging from 10.5 to
246 97.5%) whereas the model showed the average RH to be ~ 23% with values ranging between 6
247 to 78%. RH values are highly underestimated by the model, however; ~~the synoptic scale~~
248 ~~variability is adequately captured by the model~~ as previously mentioned, the model does not
249 show significant changes in RH during the measurement campaign after the observations stopped
250 working.

251 Average observed wind speed during the study period was 2.4 m s⁻¹, with hourly values ranging
252 between 0.03 - 7.4 m s⁻¹ whereas from the WRF model average wind speed was found to be 3.2
253 m s⁻¹ (range: 0.06 - 11.1 m s⁻¹). Diurnal variation of observed hourly average wind speed

254 suggested that wind speeds were lower during nights and mornings while higher wind speed
255 prevailed during day time, with average winds $> 3 \text{ m s}^{-1}$ up to $\sim 3.3 \text{ m s}^{-1}$ between 09:00-13:00
256 local time (Supplementary materials, Figure S2, lower panel). High speed strong winds ($> 4 \text{ m s}^{-1}$)
257 were from the NW direction during the month of April which later switched to almost opposite
258 direction, i.e., SE direction from the month of May onwards. ~~Figure 3 shows~~ The monthly wind
259 rose plot ~~using the data from both observation and modeling where the difference in the pattern~~
260 ~~could be potentially due to the data resolution is shown in Figure S3 (using WRPLOT view from~~
261 ~~the Lakes Environmental, <http://weblakes.com/>).~~ Comparing modeled wind direction prediction
262 skills at the surface with one point measurement is not sufficient. However, in the absence of
263 other measurements, we also show the comparison of wind direction ~~as an indication of model~~
264 ~~performance not as model validation. Since there are no glaringly large biases in the observed~~
265 ~~surface wind direction, and the lack of measured upper wind data even from nearby region, we~~
266 ~~use the model to interpret pollutant transport to Lumbini.~~ Discrepancy on model results might
267 have occurred due to various factors inherently uncertain in a weather ~~prediction using a model.~~
268 ~~Besides, air pollution transport also occurs via elevated layers and is not limited to surface~~
269 ~~winds. We show NCEP/NCAR reanalysis plots at 850 hPa in Fig. S3 to illustrate the distinctly~~
270 ~~differing wind direction compared to the surface winds seen from observations as well as~~
271 ~~NCEP/NCAR reanalysis plot at 1000 hPa shown in Fig. 1. There are no upper wind~~
272 ~~measurement data nearby Lumbini to show model performance. However~~ Regardless, we believe
273 that ~~air quality modeled~~ data is vital for understanding pollutant transport in an area where
274 observation data are non-existent or are incomplete.

275 ~~The monthly mean synoptic wind for the month of April, May and June is presented in Figure 5.~~
276 ~~NCEP/NCAR reanalysis monthly data of winds at 1000 mbar were used to study the wind~~
277 ~~pattern. The red dot in the figure indicates the location of Lumbini. NCEP/NCAR data showed~~
278 ~~the dominance of calm winds over the measurement site. Similar type of wind directions were~~
279 ~~observed over Kanpur, India, also in the IGP, during the pre-monsoon season (Srivastava et al.,~~
280 ~~2011).~~

281 3.2 Air Quality

282 3.2.1 General overview, PM ratios and influence of meteorology on pollution 283 concentrations

284 Figure 3 shows hourly averaged time series of observed BC, PM₁, PM_{2.5}, PM₁₀, ~~CO~~ and O₃ and
285 CO observed at Lumbini during the study period. Similar temporal behaviour was shown by BC,
286 particulate matter fractions (PM₁, PM_{2.5} and PM₁₀) and CO. The gap in the figure (for PM time
287 series) is due to the power interruption to the instrument. BC concentrations during the
288 measurement period ranged between 0.3-29.9 $\mu\text{g m}^{-3}$ with a mean ($\pm\text{SD}$) value of 4.9 (± 3.8) μg
289 m^{-3} . BC concentrations in Lumbini during pre-monsoon months are lower compared to BC
290 concentrations observed in the Kathmandu Valley because of high number of vehicles plying on
291 the street, brick kilns and other industries in Kathmandu valley (Sharma et al., 2012;Putero et al.,
292 2015). The lowest concentration was observed during a rainy day (21-22 April) whereas the
293 highest concentration was observed during a period of forest fire (detailed in Section 3.4 3.3).
294 For the entire measurement period, we found average (of hourly average values) PM₁: 35.8 \pm 25.6
295 $\mu\text{g m}^{-3}$ (minimum-maximum range: 3.6 - 197.6 $\mu\text{g m}^{-3}$), PM_{2.5}: 53.1 \pm 35.1 $\mu\text{g m}^{-3}$ (6.1 - 272.2 μg
296 m^{-3}), PM₁₀: 128.9 \pm 91.9 $\mu\text{g m}^{-3}$ (10.5-603.9 $\mu\text{g m}^{-3}$) and coarse-mode (PM_{10-2.5}): 75.65 \pm 61.67 μg
297 m^{-3} (1.98-331.80 $\mu\text{g m}^{-3}$). The coarse-mode fraction was ~ 60% of the PM₁₀. The share of coarse-
298 mode aerosol to PM₁₀ in Lumbini was higher than that observed in other sites in the IGP;
299 Guwahiti, India (42%) (Tiwari et al., 2017) and Dibrugarh, India (9-16%) (Pathak et al., 2013)
300 both in eastern IGP and Delhi (38%) (Tiwari et al., 2015) in western IGP indicating the higher
301 contribution of coarse aerosols in Lumbini, likely lifted from soils from nearby agricultural fields
302 and construction materials by stronger winds during pre-monsoon season. Similar value of
303 coarse-mode fraction, as in Lumbini, has been reported by Misra et al. (2014) at Kanpur for dust
304 dominated and mixed aerosols events.

305 The share of BC in PM fractions were found to be ~13% in PM₁, 9% in PM_{2.5} and ~4% in PM₁₀
306 but the correlation coefficients of BC with three PM fractions were found to be 0.89 (PM₁), 0.88
307 (PM_{2.5}) and 0.69 (PM₁₀), indicating the commonality in the sources of these pollutants. The
308 contribution of BC in PM₁ was found to be of ~12% in Kanpur during February-March (Kumar
309 et al., 2016a) similar to Lumbini. Regarding the share of BC in PM₁₀, the share observed in
310 Lumbini (~4%) was similar to that observed over Varanasi (~340 km due south of our site) in
311 central IGP (5%) (Tiwari et al., 2016) and Dibrugarh in eastern IGP (~5%) (Pathak et al., 2013).

312 Thus our results indicate that despite our station being located at the northern edge of the IGP
313 along the foothills of the Himalayan range, its aerosol characteristics are similar to those found in
314 heavily polluted sites in the central and eastern IGP.

315 In Lumbini, the average (hourly) share of PM_1 in $PM_{2.5}$, PM_1 in PM_{10} and $PM_{2.5}$ in PM_{10} were
316 found to be ~70%, 34% and 47% respectively. The share of average (sampling period) coarse-
317 mode aerosols to PM_{10} (60%) was found to be higher as compared to that of average fine mode
318 i.e., $PM_{2.5}$ (40%). Regarding other sites in IGP region, $PM_{2.5}/PM_{10}$ ratios were reported to be
319 56% in Kanpur (Snider et al., 2016), 60% in Varanasi (Kumar et al., 2015), 57% in Guwahiti
320 (Tiwari et al., 2017), 90% in Dribugarh (Pathak et al., 2013) and 62% in Delhi (Tiwari et al.,
321 2015) indicating local differences within IGP as well as suggesting that influence of combustion
322 sources at Lumbini is still lower compared to other locations in Indian section of the IGP. A
323 recent study (Putero et al., 2015) reported the PM_1/PM_{10} during pre-monsoon of 2013 was found
324 to be 0.39 in the Kathmandu Valley of Nepal. Lumbini has significantly lower vehicle emissions
325 and human population than the Kathmandu Valley yet the ratios are similar, indicating the
326 importance of regional combustion sources in Lumbini for finer aerosols (PM_1), and soil-based
327 emissions such as road dust in the Kathmandu Valley. Future studies will need to explore the
328 emission sources around Lumbini in much greater detail. Lower $PM_{2.5}/PM_{10}$ in Lumbini as
329 compared to other regions mentioned earlier could be due to emissions from cement industries
330 located within 15 km distance from the measurement site. Cement factories emit coarse sized
331 particles but we are not able to distinguish in our measurement without having an analysis of
332 certain marker species. Trivedi et al. (2014) reported a ratio of 0.39 (during pre-monsoon) over
333 Delhi, which is lower than the ratio in Lumbini. The lower ratio in Delhi was due to the presence
334 of coarse sized windblown desert dust and suspended soil materials due to strong winds.

335 The observed 24-hour average particulate matter concentrations ($PM_{2.5}$ and PM_{10}) were found
336 frequently higher than the WHO prescribed guidelines for $PM_{2.5}$ ($25 \mu\text{g m}^{-3}$) and PM_{10} ($50 \mu\text{g m}^{-3}$)
337 with $PM_{2.5}$: exceeding 94% and PM_{10} : 85% of the measurement period of 53 days in
338 **Lumbini**.

339 Observed CO concentrations ranged between 124.9-1429.7 ppbv with an average value of
340 344.1 ± 160.3 ppbv. CO concentration observed in Lumbini is lower than that of Mohali, Western
341 India where the average concentration was 566.7 ppbv during pre-monsoon season due to intense

342 biomass and agro-residue burning over the region (Sinha et al., 2014). Temporal variation of CO
343 concentrations is similar to that of BC as both of these species are emitted during incomplete
344 combustion of fuel. Moreover, a very strong correlation ($r = 0.9$) was observed between BC and
345 CO. Past studies have shown that the ratio of BC to CO depends upon multiple factors like site
346 location, combustion characteristics (fuel and technology) at the sources, and type of air mass
347 (Girach et al., 2014; Pan et al., 2011; Zhou et al., 2009). Formation of the soot depends on the
348 carbon to oxygen ratio of fuel whereas CO can also be produced naturally due to the oxidation of
349 VOCs (Girach et al., 2014). Figure 4 shows the comparison of the average $\Delta BC/\Delta CO$ ratio
350 (0.021) at Lumbini with that obtained from other sites. Please refer to Figure S4 in the
351 supplementary materials for the time series of $\Delta BC/\Delta CO$ ratio observed in Lumbini. We used the
352 method described by Pan et al. (2011) to calculate the $\Delta BC/\Delta CO$ values. The ratio was
353 calculated using the equation $(BC - BC_0)/(CO - CO_0)$ assuming the background values (BC_0 or
354 CO_0) as 1.25 percentile of the data. The $\Delta BC/\Delta CO$ ratio in Lumbini is similar to that obtained at
355 a suburban site, Pantnagar in India (0.017) (Joshi et al., 2016) and in Maldives (0.017)
356 (Dickerson et al., 2002). As compared to Lumbini, the different $\Delta BC/\Delta CO$ ratio obtained over
357 megacities such as Beijing and Shanghai are due to the higher number of gasoline and diesel
358 vehicles (Zhou et al., 2009). However, the ratio obtained at Lumbini were within the range of
359 emission ratios from diesel used in transport sector (0.0013-0.055), coal (0.0019-0.0572) and
360 biofuels (0.0087-0.0266) for domestic activities (Verma et al., 2010 and references therein). The
361 hourly averaged observed ozone concentration ranged between 1.0 and 118.1 ppbv with a mean
362 value of 46.6 ± 20.3 ppbv during the sampling period. The 8-hr maximum O_3 concentration
363 exceeded WHO guidelines of $100 \mu g m^{-3}$ (WHO, 2006) during 88% of the measurement period.
364 Our results clearly indicate that the current pollution levels in Lumbini is of great concern to
365 health of the people living in the region as well as over a million visitors who visit Lumbini, as
366 well as ecosystems, particularly agro-ecosystem, especially in warm and sunny pre-monsoon
367 months.

368 The relationship of wind speed (WS) with aerosol and gaseous pollutants in Lumbini is shown in
369 Figure S5 (Supplementary information). We were interested in studying the relationship between
370 wind speed and the pollutants since the wind governs the horizontal dilution of the pollutants
371 (Huang et al., 2012) and also likelihood of lifting soil dust. Except ozone, all other pollutants

372 exhibited negative correlation with wind speed. BC shows negative correlation ($r = -0.42$) with
373 the wind speed which is similar with other pollutants as well (as can be seen from the figure).
374 Past studies have also reported a similar negative correlation of BC with wind speed over urban
375 and sub-urban areas (Huang et al., 2012;Cao et al., 2009;Ramachandran and Rajesh,
376 2007;Sharma et al., 2002;Tiwari et al., 2013) indicating that the locally generated BC can
377 accumulate in the atmosphere during lower wind speed conditions (Cao et al., 2009). Tiwari et
378 al. (2013) also reported similar negative correlation ($r = -0.45$) during the pre-monsoon season
379 over Delhi. On the other hand, secondary pollutants like ozone exhibited a positive relation with
380 the WS ($r=0.38$) indicating the WS could be one of the potential factors of high ozone in
381 Lumbini. Solar radiation is one of the most important factors for production of ozone in the
382 atmosphere (Naja et al., 2003). The correlation of hourly ozone concentration with solar
383 radiation (not shown here) was found to be 0.41 whereas wind speed during the daytime only
384 (06:00-18:00) showed very weak correlation of 0.02 with ozone, indicating the calm condition as
385 conducive to formation and accumulation of ozone in the region.

386 Interestingly, the highest concentrations of all measured pollutants were obtained when the wind
387 speed was less than 1 m s^{-1} . In a separate analysis (not shown here), we considered only the WS
388 $>1 \text{ m s}^{-1}$ and calculated the correlation coefficients to investigate the influence of regional
389 emissions. We found the similar correlation values as previous when all WS values were
390 considered (BC vs WS = -0.41, CO vs WS = -0.42, O₃ vs WS= 0.29, PM₁ vs WS= -0.40, PM_{2,5}
391 vs WS= -0.38, PM₁₀ vs WS= -0.33). The correlation of WS ($>1 \text{ m/s}$) with concentration of air
392 pollutants elucidates that air pollution over Lumbini is not only of the local origin, it is rather
393 transported from other nearby regions as well.

394 Past studies near this site have been focused on the cities like Kathmandu (Sharma et al.,
395 2012;Ram et al., 2010;Panday and Prinn, 2009;Putero et al., 2015) and Kanpur (Ram et al.,
396 2010) and agro-residue burning dominated regions of IGP (Rastogi et al., 2016;Sinha et al.,
397 2014;Sarkar et al., 2013) or a remote mountain location in India (Naja et al., 2014). Very high
398 aerosol loading is observed in South Asia during pre-monsoon, mostly over the IGP region
399 (Supplementary materials, Figure S6). As this is the first study over an IGP site located in Nepal,
400 pollution concentrations observed at Lumbini were compared with other sites in the region
401 (Table 2). Different sites located at urban, semi-urban and remote locations were used for

402 comparison to get a clear comparative picture of the situation at Lumbini amongst other locations
403 in the region. Pre-monsoon seasonal average PM_{2.5} concentration in Lumbini has been found to
404 be lower than the megacity like Delhi (Bisht et al., 2015) and north-western IGP (Sinha et al.,
405 2014), possibly due to higher level of emissions (from traffic and biomass burning, respectively)
406 over those regions. In addition, average BC and CO concentrations in Lumbini were found
407 falling in between concentrations observed at rural sites (up to 6 times higher) and cities in the
408 region (see Table 2), indicating that Lumbini, **in a way**, can still be considered as semi-urban
409 location. The hourly average O₃ concentration in Lumbini were found to be higher than the cities
410 like Kathmandu (Putero et al., 2015) and Kanpur during pre-monsoon season (Gaur et al., 2014).
411 However from a mesoscale perspective, the hourly average O₃ concentrations were lower at
412 Lumbini as compared to base camp of Mt. Everest region due to the uplift of polluted air masses
413 (Marinoni et al., 2013), stratospheric intrusion (Cristofanelli et al., 2010) and even the regional
414 or long-range transport of the air pollutants (Bonasoni et al., 2010) to the high altitude site.
415 Regarding the monthly average concentration, the concentrations of all measured pollutants
416 decreased as the pre-monsoon months advanced. The monthly average concentrations of the
417 monitored species are shown in the Figure S7 along with the monthly fire hotspots over the
418 region. Reduction in concentration (except PM) during the month of May (as compared to April)
419 could be attributed to the fewer fire events during May as well as previously discussed washout
420 by rainfall. Two peak pollution episodes were observed during the first half of April and May
421 which is discussed in more detail in the next section.

422 **3.2.2 Observation-model inter-comparison**

423 Chemical transport models provide insight to observed phenomena; however, interpretation has
424 to take into account model performance before arriving at any conclusion. This section describes
425 pollution concentrations simulated by the WRF-STEM model. A comparison of model calculated
426 pollutant concentration along with the minimum and maximum concentrations of various
427 pollutants (with observation) is shown in Table 3. The model based concentrations used here are
428 instantaneous values for every third hour of the day. BC concentrations ranged between 0.4-3.7
429 $\mu\text{g m}^{-3}$ with a mean value of $1.8\pm 0.7 \mu\text{g m}^{-3}$ for a period of 1st April-15th June 2013. The average
430 model BC concentration was ~ 2.7 times lower than the observed BC. Regarding PM₁, PM_{2.5} and
431 PM₁₀, the model simulated average concentration was 12.3 ± 5.5 (0.9-41.7) $\mu\text{g m}^{-3}$, 17.3 ± 6.7 (1.9-

432 48.3) $\mu\text{g m}^{-3}$ and 25.4 ± 12.9 (2.1-68.8) $\mu\text{g m}^{-3}$, respectively. The model estimated values were
433 lower by the factor of 3 and 5 respectively than the observed concentrations. The data show that
434 model needs much improvement in its ability to adequately predict observed aerosol
435 characteristics at Lumbini. Since pollutant concentration is a function of emissions, transport and
436 transformation and deposition, improvements in any of these areas would improve the model.
437 However, given observation insights by PM ratios, it seems that improvements are much needed
438 in the emissions of primary aerosols. Current emissions does not account for trash burning,
439 roadside dust and increasingly newer industries, especially emissions from cement factories that
440 have propped up in recent years.

441 Average observed CO concentration was 255.7 ± 83.5 ppbv, ranging between 72.2-613.1 ppbv,
442 with average model CO ~ 1.35 times lower than observed. Time series comparison of modeled
443 CO versus observation is shown in Figure 3. Apart from two peak episodes the model does a
444 better job in predicting CO concentration over Lumbini. Previous study using the STEM model
445 over Kathmandu valley showed that the model was able to capture annual BC mean value but
446 completely missed the concentrations during pre-monsoon and post monsoon period (Adhikary
447 et al., 2007). Similar behavior is seen this time for CO where the model misses the peak values
448 but reasonably captures CO concentration after mid-May when no biomass burning events are
449 observed (model to observation ratio improves to 1.16). STEM model CO performance can be
450 significantly improved via better constraining emissions of open biomass burning as discussed in
451 Section 3.3. This activity is beyond the scope of this current paper although the improvements
452 are underway for all these sectors.

453 3.2.3 Diurnal variations of air pollutants and boundary layer height

454 In the emission source region, diurnal variations of primary pollutants provide information about
455 the time dependent emission activities (Kumar et al., 2016b). Figure 5 shows the diurnal
456 variation of hourly averaged concentrations of measured pollutants during the sampling period.
457 Primary pollutants like BC, PM and CO showed typical characteristics of an urban environment,
458 i.e., diurnal variation with a morning and an evening peak. However, Lumbini data shows higher
459 concentrations in the evenings compared to morning hours. Elevated concentrations can be
460 linked to morning and evening cooking hours for BC and CO where emission inventory show
461 that residential sector has significant contribution. However, explanation for elevated evening

462 concentration compared to morning needs further investigation. Increase in the depth of
463 boundary layer, reduction in the traffic density on the roads, absence of open biomass burning
464 during mid-day and increasing wind speed often contribute to the dispersion of pollutants
465 resulting in lower concentration during afternoon. Diurnal variation of wind direction
466 (Supplementary information, Figure S2, upper panel) shows the dominance of wind coming from
467 south (mainly during the month of May and till mid-June). Morning and evening period
468 experienced the winds coming from the southeast direction while the winds were predominantly
469 from southwest direction during late afternoon. Increase in CO concentrations in the evening
470 hours might be due to transport of CO from source regions upwind of Lumbini which along with
471 the local emissions ~~which~~ gets trapped under ~~lower reduced~~ Planetary Boundary Layer (PBL)
472 heights ~~in evening and night time~~. Ozone concentration was lowest in the morning before the
473 sunrise and highest in late afternoon around 15:00 PM after which concentrations started
474 declining, exhibiting a typical characteristic of a polluted urban site. Photo-dissociation of
475 accumulated NO_x reservoirs (like HONO) provides sufficient NO concentration leading to the
476 titration of O₃ resulting in minimum O₃ just before sunrise (Kumar et al., 2016b). The PBL
477 height (in meters (m)) was obtained from the WRF model as observations were not available.
478 ~~Figure 7 shows the monthly diurnal variation of the model derived PBL height.~~ The study period
479 average PBL height over Lumbini was ~ 910 m (ranging between 24.28 and 3807 m observed at
480 06:00 and 15:00 respectively). ~~The daily average PBL height obtained from the model is~~
481 ~~compared with published values (Wan et al., 2017) as shown in Figure 6, which indicate that the~~
482 ~~value is captured by our model during initial measurement period and overestimated in the~~
483 ~~months of mid May onwards.~~ As the pre-monsoon month advances, PBL height also increased.
484 The monthly average PBL height was 799 m, 956 m and 1014 m respectively during the month
485 of April, May and (1st-15th) June. ~~As presented in the figure, the monthly average diurnal~~
486 ~~variation also showed that the boundary layer height was maximum during 15:00 local time~~
487 ~~during each month which coincides with the period of lowest concentration of the pollutants.~~ ~~The~~
488 ~~fluctuations of modeled PBL height correspond well with the diurnal variation of observed~~
489 ~~pollutants like BC, CO and PM with the period of lower boundary height experiencing higher~~
490 ~~pollution concentration.~~

491 3.3 Influence of forest fires on Lumbini air quality

492 3.3.1 Identification of forest fire influence over large scale using in-situ observations 493 satellite and model data

494 Forest fires and agricultural biomass burning (mostly agro-residue burning in large scale) are
495 common over the South Asia and the IGP region during pre-monsoon season. North Indo-
496 Gangetic region is characterized by fires even during the monsoon and post-monsoon season
497 (Kumar et al., 2016b;Putero et al., 2014). These activities influence air quality not only over
498 nearby regions but also get transported towards high elevation pristine environments like Mt.
499 Everest (Putero et al., 2014) and Tibet (Cong et al., 2015a;2015b). So, one of the main objectives
500 of this study was to identify the influence of open burning on Lumbini air quality. Average wind
501 speed during the whole measurement period was 2.4 m s^{-1} . Based on this data, open fire counts
502 within the grid size of $200 \times 200 \text{ km}$ centering over Lumbini was used for this analysis assuming
503 that the emissions will take a maximum period of one day to reach our monitoring site. Forest
504 fire counts were obtained from MODIS satellite data product ~~called Global Monthly Fire~~
505 ~~Location Products-MCD14ML~~ **Fire Information for Resource Management System (FIRMS)**.
506 More on this product has already been described by Putero et al. (2014). Figure 7 shows the daily
507 average $\Delta\text{BC}/\Delta\text{CO}$ ratio, aerosol absorption Ångstrom exponent (AAE) which is derived from
508 Aethalometer data and daily open fire count within the specified grid. The green box in the
509 figure is used to show two peak events (presented earlier in Fig. 3) with the elevated BC and CO
510 concentrations observed during the monitoring period. The first peak was observed during 7-9
511 April and second peak during 3-4 May, 2013. Two pollutants having biomass burning as the
512 potential primary source: BC and CO were taken in consideration. **High** AAE values (~ 1.6)
513 **higher** during these two events (~~~ 1.6~~) are also an indication of presence of BC of biomass
514 burning origin. The chemical composition of TSP filter samples collected at Lumbini also
515 showed higher concentration of Levoglucosan, a biomass burning tracer in Lumbini during the
516 pre-monsoon season as compared to other seasons of the year (Wan et al., 2017). Wan et al.
517 (2017) also reported that the higher correlation between K^+ with tracers of dust (Ca^{2+} and Mg^{2+})
518 indicated that dust is the main source of potassium in Lumbini.

519 Contrary to our expectation, we could not observe any significant influence of forest fire within
520 the specified grid of $200 \times 200 \text{ km}$ (or the influence of local forest fire on the air quality over
521 Lumbini was not observed). Therefore, a wider area, covering South and Southeast Asian

522 regions, was selected for the forest fire count. Figure 8 (A-B) shows the active fire hotspots from
523 MODIS, over the region, during the peak events which shows the first peak **could have** occurred
524 due to the forest fire over the eastern India region whereas the second peak was influenced by the
525 forest fire over western IGP region. Moreover, in order to strengthen our hypothesis, we have
526 utilized satellite data products for various gaseous pollutants like CO and NO₂ (Atmospheric
527 Infrared Sounder (AIRS) for CO and Ozone Monitoring Instrument (OMI) for NO₂ both
528 obtained from Giovanni platform). Figure 8 (C-H) shows the daytime total column CO before,
529 during and after occurrence of two events (peaks) as stated earlier. Atmospheric Infrared
530 Sounder (AIRS) satellite with daily temporal resolution and 1°×1° spatial resolution have been
531 utilized to understand the CO concentration over the area. CO concentration over Lumbini
532 during both of the peaks confirmed the role of open fires ~~on either sides of~~ **over** the IGP region
533 for elevated concentration of CO in Lumbini. To further strengthen our finding, the aid of
534 **HYSPLIT back trajectories plots** ~~of local wind speed and direction~~ was taken. Figure 8 (I-J)
535 represent the **6-hourly back trajectories** ~~wind rose plot~~ only for these two events respectively.
536 **However, the back trajectories (during both events) indicated that the air mass passed over the**
537 **fire events in the north western IGP. We note that using back trajectories to identify source**
538 **regions are also uncertain as identified by Jaffe et al. (1997).** ~~Wind rose plots also confirm the~~
539 ~~wind blowing from those two forest fire regions affected the air quality in Lumbini region.~~
540 Figure 8 (K) shows model biomass CO peak coincident with observed CO. Although the
541 magnitudes are significantly different, the timing of the peaks is well captured by the model.
542 This, we believe, is due to the fact that satellite based open fire detection also has limitation as it
543 does not capture numerous small fires that are prevalent over south Asia which usually burn out
544 before the next satellite overpass. More research is needed to assess the influence of these small
545 fires on regional air quality.

546 In a separate analysis (not shown here), elevated O₃ concentration during these two events were
547 also observed. Average O₃ concentration before, during and after the events were found to be
548 46.2±20.3 ppbv, 53.5±31.1 ppbv and 50.3±20.9 ppbv respectively (Event-I) whereas it was
549 found to be 54.8±23.8 ppbv, 56.7±35 ppbv and 55.6±13.4 ppbv respectively (Event-II).
550 Increased ozone concentrations during the high peak events have been analyzed using the
551 satellite NO₂ concentration over the region considering the role of NO₂ as precursor for ozone

552 formation. Daily total column NO₂ were obtained from OMI satellite (data available at the
553 Giovanni platform; <http://giovanni.gsfc.nasa.gov/giovanni/>) at the spatial resolution of
554 0.25°×0.25°. Figure 9 shows the NO₂ column value before, during and after both events. Even for
555 the NO₂, maximum concentrations were observed during these two special events. **It is likely that
556 the local as well as regional pollution (transported from NW IGP region as indicated by synoptic
557 wind in Figure S8) contributed to the ozone peak. However, we are not able to quantify the
558 individual contributions, even with the model simulation, because ozone was not simulated in
559 this experiment.**

560 **3.3.2 Identifying regional and local contribution**

561 WRF-STEM model has been used to identify the anthropogenic emission source region
562 influencing the air quality over Lumbini. As previously explained, the model is able to capture
563 the observed CO concentration when intense open burning events were not present. A recent
564 study (Kulkarni et al., 2015) has explored the source region contribution of various pollutants
565 over the Central Asia using similar technique. Figure 10 (A) shows the average contribution
566 from different regions on CO concentration over Lumbini during the whole measurement period.
567 Major share of CO was from the Ganges valley (46%) followed by Nepal region (25%) and rest
568 of Indian region (~17.5%). Contribution from other South Asian countries like Bangladesh and
569 Pakistan were ~ 11% whereas China contributed for ~1% of the CO concentration in Lumbini.
570 Regarding the monthly average contribution, the Ganges Valley and Nepal's contribution were
571 almost equal during the month of April (~34% and ~37% respectively) but increased for the
572 Ganges Valley region during the month of May (~44%) and got reduced for Nepal region
573 (~25%) (Figure S9).

574 Figure 10 (B) is the time series of percentage contribution to total CO concentration during
575 whole measurement period showing different air mass arriving at a 3 hourly intervals. During the
576 whole measurement period, majority of the CO reaching Lumbini were from the Ganges valley
577 (mainly the states of Punjab, Haryana, Uttar Pradesh, Bihar and West Bengal) region with the
578 contribution sometimes reaching up to ~80%. Other India (central, south, east and north) regions
579 also contributed significantly. Bangladesh's contribution in CO loading was seen only after mid-
580 April lasting for only about a week and after the first week of May. The contribution from
581 Bangladesh was sporadic comparing to other regions. Highest contribution from this Bangladesh

582 region was observed after the first week of June with the arrival of monsoonal air mass. Pakistan
583 also contributed for the CO loading significantly. Others region as mentioned in the figure
584 covered the regions like Afghanistan, Middle east, West Asia, East Asia, Africa and Bhutan.
585 Contributions from these regions were less than 5%. Contribution from China was not evident
586 till the first week of June where a specific air mass arrival shows contribution reaching up to
587 25% of total CO loading.

588 A sensitivity analysis was performed for emission uncertainty in the model grid containing
589 Lumbini. Lumbini and surrounding regions in the recent years has seen significant rise in urban
590 activities and industrial activity and related emissions which may not be accurately reflected in
591 the HTAPv2 emissions inventory. A month long simulation was carried out with emissions from
592 Lumbini and the surrounding four grids off and another simulation with Lumbini and
593 surrounding four grid's emissions increased by 5 times the amount from HTAPv2 emissions
594 inventory. The results are shown in Figure 10 (C) as percentage increase or decrease compared
595 to model results using the current HTAPv2 emissions inventory. The black line shows
596 concentration as 100% for the current HTAPv2 emissions inventory. Despite making Lumbini
597 and the surrounding grids emissions zero, model calculation shows pollutant concentration on
598 average is still about 78% of the original value indicating dominance of background and regional
599 sources compared to local source in the model. Increasing emissions 5 times for the Lumbini and
600 surrounding four grids only increases the concentration on average by 151%. Thus uncertainty in
601 emissions are not a local uncertainty for Lumbini rather for the whole region which needs to be
602 better understood for improving model performance against observations at Lumbini.

603 **3.4 Does fossil fuel or biomass influence the Lumbini air?**

604 The aerosol spectral absorption is used to gain insight into nature and potential source of black
605 carbon. This method enables to analyze the contributions of fossil fuel combustion and biomass
606 burning contributions to the observed BC concentration (Kirchstetter et al., 2004). Besides BC,
607 other light absorbing (in the UV region) aerosols are also produced in course of combustion,
608 collectively termed as organic aerosols (often also called brown carbon or BrC) (Andreae and
609 Gelencsér, 2006). Figure 11 shows the comparison of normalized light absorption as function of
610 the wavelength for BC observed at Lumbini during cooking and non-cooking hours **and also for**
611 **the both events**. Our results are compared with the published data of Kirchstetter et al. (2004)

612 and that observed over a village center site of Project Surya in the IGP (Praveen et al., 2012)
613 (figure not shown). We discuss light absorption data from two distinct times of the day. The
614 main reason behind using data during 07:00-08:00 h and 16:00-17:00 h is these periods represent
615 highest and lowest ambient concentration (Fig. 5). Also these period represent cooking and non-
616 cooking or high and low vehicular movement hours (Praveen et al., 2012). To understand the
617 influence of biomass and fossil fuel we plotted normalized aerosol absorption at 700 nm
618 wavelength for complete aethalometer measured wavelengths in Fig. 11. Kirchstetter et al.
619 (2004) reported OC absorption efficiency at 700 nm to be zero. Thus we normalized measured
620 absorption spectrum by 700 nm wavelength absorption. Since aethalometer does not provide 700
621 nm wavelength absorption values, we used methodology followed by Praveen et al. (2012). Our
622 results show that the normalized absorption for biomass burning aerosol is ~3 times higher at
623 370 nm compared to that at 700 nm whereas fossil fuel absorption is about 2.6 times higher at
624 the same wavelength. **In addition, the curve obtained for the both events are inclined towards the**
625 **published biomass burning curve.** The normalized curve obtained during both cooking and non-
626 cooking period lies in between the standard curve of Kirchstetter et al. (2004). As shown in Fig.
627 11, the curve obtained for the prime cooking time is closer towards the published curve on
628 biomass burning whereas that obtained during the non-cooking time is closer towards the
629 published fossil fuel curve. Similar result was also observed over the Project Surya village in the
630 IGP region (Praveen et al., 2012;Rehman et al., 2011). This clearly indicates there is contribution
631 of both sources: biomass as well as fossil fuel on the observed BC concentration over Lumbini.

632 In order to identify fractional contribution of biomass burning and fossil fuel combustion to
633 observed BC aerosol, we adopted the method described by Sandradewi et al. (2008). Wavelength
634 dependence of aerosol absorption coefficient (b_{abs}) is proportional to $\lambda^{-\alpha}$ where λ is the
635 wavelength and α is the absorption Ångstrom exponent. The α values ranges from 0.9-2.2 for
636 fresh wood smoke aerosol (Day et al., 2006) and between 0.8-1.1 for traffic or diesel soot
637 (references in Sandradewi et al. (2008)). We have taken α value of 1.86 for biomass burning and
638 1.1 for fossil fuel burning as suggested by previous literature (Sandradewi et al., 2008). Figure
639 12 shows diurnal variation of the biomass burning BC. Minimum contribution of biomass
640 burning to total BC concentration was observed during 04:00-06:00 local time (only about 30%
641 of the total BC). As the cooking activities start in morning, the contribution of biomass BC starts

642 to increase and reaches about 50%. Similar pattern was repeated during evening cooking hours.
643 Only during these two cooking periods, fossil fuel fraction BC was lower. Otherwise it remained
644 significantly higher than biomass burning BC throughout the day. On average, ~40% of BC was
645 from biomass burning whereas remaining 60% was contributed by fossil fuel combustion during
646 our measurement period. Interestingly, this is the opposite of the contributions that were
647 concluded by Lawrence and Lelieveld (2010). Lawrence and Lelieveld (2010) concluded that
648 ~60% BC from biomass versus ~40% fossil fuel, based on a review of numerous previous
649 studies to be likely for the outflow from Southern Asia during the winter monsoon. When we
650 compared observed Ångström exponent with Praveen et al. (2012), we noticed that Lumbini
651 values were lower than Project Surya Village center site. This implies Surya village center had
652 higher biomass fraction, also it was observed absorption Ångström exponent exceeded 1.86
653 during cooking hours which indicates 100% biomass contribution. The difference is attributed to
654 the fact that Lumbini sampling site is not a residential site like Surya village which can capture
655 cooking influence efficiently. Further Lumbini sampling site is surrounded by commercial
656 activities such as a local bus park, hotels, office buildings and industries and brick kilns slightly
657 further away. Although the reason for this difference is not clear, it is an indication of the
658 important role of diesel and coal emissions in the Lumbini and upwind regions.

659 4. **Conclusions**

660 Our measurements, a first for the Lumbini area, have shown very high air pollution concentration
661 at Lumbini. Black carbon (BC), carbon monoxide (CO), ozone (O₃) and particulate matter
662 (PM₁₀, PM_{2.5} and PM₁) were measured during the pre-monsoon of 2013 as a regional site of the
663 *SusKat-ABC campaign*. Average pollutant concentrations during the monitoring period were
664 found to be: BC: $4.9 \pm 3.8 \mu\text{g m}^{-3}$; CO: $344.1 \pm 160.3 \text{ ppbv}$; O₃: $46.6 \pm 20.3 \text{ ppbv}$; PM₁₀: 128.8 ± 91.9
665 $\mu\text{g m}^{-3}$ PM_{2.5}: $53.14 \pm 35.1 \mu\text{g m}^{-3}$ and PM₁: $36.6 \pm 25.7 \mu\text{g m}^{-3}$ which is comparable with other
666 urban sites like Kanpur and Delhi in the IGP region. However, our study finds higher fraction of
667 coarse mode PM in Lumbini as compared to other sites in the IGP region. In addition, $\Delta\text{BC}/\Delta\text{CO}$
668 ratio obtained in Lumbini was within the range of emission from both domestic residential and
669 transportation sectors, indicating them as potential key sources of BC and CO, and likely most of
670 PM₁ in Lumbini. The diurnal variation of the pollutants is similar to that of any urban location,

671 with peaks during morning and evening. However, our results show higher evening
672 concentration compared to morning concentration values and needs further research to explain
673 this behavior. During our measurement period, air quality in Lumbini was influenced by regional
674 forest fires as shown by chemical transport model and satellite data analysis. A regional chemical
675 transport model, WRF-STEM was used to **interpret understand** observations. Inter-comparison of
676 WRF-STEM model outputs with observations showed that the model underestimated the
677 observed pollutant concentrations by a factor of ~1.5 to 5 but was able to capture the temporal
678 variability. Model uncertainties are attributed mostly to uncertainties in meteorology and
679 regional emissions as shown from sensitivity analysis with local emissions. Region-tagged CO as
680 air-mass tracers are employed in WRF-STEM model to understand the anthropogenic emission
681 source region influencing Lumbini. Our analysis shows that the adjacent regions; mostly the
682 Ganges valley, other parts of India and Nepal accounted for the highest contribution to pollutant
683 concentration in the Lumbini. The normalized light absorption curve clearly indicated the
684 contribution to BC in Lumbini from both sources: biomass as well as fossil fuel. On average,
685 ~40% BC was found to be from the biomass burning and ~60% from fossil fuel burning.
686 Various improvements and extensions would be possible in future studies. More reliable
687 functioning of the AWS (temperature and RH sensor, rain gauge) would have allowed more in-
688 depth analysis of the relationship between meteorological parameters and pollutants
689 concentration. Continuous measurements of air pollutants throughout the year would allow for
690 annual and seasonal variation study. Improvements in the model are much needed in its ability to
691 simulate observed meteorology. Significant uncertainty lies with regional emissions inventory
692 developed at national and continental scale versus local bottoms up inventory and pollutant
693 emissions from small scale open burning not captured by satellites. There is a clear need for
694 setting up of a continuous air quality monitoring station at Lumbini ([UNESCO World Heritage](#)
695 [Site](#)) and the surrounding regions for long-term air quality monitoring.

696 **Data availability**

697 The data used for this manuscript can be obtained by sending an email to the corresponding
698 authors and/or to IASS (Maheswar.Rupakheti@iass.potsdam.de) and/or to ICIMOD
699 (arnico.panday@icimod.org). Modeling data can be obtained from B. Adhikary
700 (Bhupesh.adhikary@icimod.org).

701 **Authors' contributions**

702 M.R. and M.L. conceived the Lumbini portion of the SusKat experiment. M.R. and A.K.P.
703 coordinated the Lumbini field campaign. D.R. and K.S.M conducted the field observations at
704 Lumbini. B.A. designed and ran the WRF-STEM model. P.S.P., B.A. and D.R. finalized the
705 manuscript composition. D.R., P.S.P, B.A., M.R. and S.K. conducted the data analysis. D.R. and
706 B.A. prepared the manuscript with inputs from all coauthors.

707 **Acknowledgements**

708 This study was partly supported by the Institute for Advanced Sustainability Studies (IASS),
709 Germany, the International Centre for Integrated Mountain Development (ICIMOD), and the
710 National Natural Science Foundation of China (41121001, 41225002), and the Strategic Priority
711 Research Program (B) of the Chinese Academy of Sciences (XDB03030504). Dipesh Rupakheti
712 is supported by CAS-TWAS President's Fellowship for International PhD Students. The IASS is
713 grateful for its funding from the German Federal Ministry for Education and Research (BMBF)
714 and the Brandenburg Ministry for Science, Research and Culture (MWFK). ICIMOD authors
715 would like to acknowledge that this study was partially supported by core funds of ICIMOD
716 contributed by the governments of Afghanistan, Australia, Austria, Bangladesh, Bhutan, China,
717 India, Myanmar, Nepal, Norway, Pakistan, Switzerland, and the United Kingdom. The views and
718 interpretations in this publication are those of the authors and are not necessarily attributable to
719 the institutions they are associated with. We thank B. Kathayat, B.R. Bhatta, and Venerable
720 Vivekananda and his colleagues (Panditarama Lumbini International Vipassana Meditation
721 Center) for providing logistical support which was vital in setting up and running the site. We
722 also thank C. Cüppers and M. Pahlke of the Lumbini International Research Institute (LIRI) for
723 proving the space and power to run the instruments at the LIRI premises. Satellite data providers
724 (MODIS, AIRS, OMI) and HYSPLIT team are also equally acknowledged.

725

726 **References**

- 727 Adhikary, B., Carmichael, G. R., Tang, Y., Leung, L. R., Qian, Y., Schauer, J. J., Stone, E. A.,
728 Ramanathan, V., and Ramana, M. V.: Characterization of the seasonal cycle of south Asian
729 aerosols: A regional-scale modeling analysis, *Journal of Geophysical Research*, 112,
730 D22S22, 1-22, 10.1029/2006jd008143, 2007.
- 731 Andreae, M. O., and Gelencsér, A.: Black carbon or brown carbon? The nature of light-
732 absorbing carbonaceous aerosols, *Atmos. Chem. Phys.*, 6, 3131-3148, doi: 10.5194/acp-6-
733 3131-2006, 2006.
- 734 Baedecker, P. A., Reddy, M. M., Reimann, K. J., and Sciammarella, C. A.: Effects of acidic
735 deposition on the erosion of carbonate stone — experimental results from the U.S. National
736 Acid Precipitation Assessment Program (NAPAP), *Atmos. Environ.*, 26, 147-158, doi:
737 10.1016/0957-1272(92)90018-N, 1992.
- 738 Bergin, M. H., Tripathi, S. N., Jai Devi, J., Gupta, T., McKenzie, M., Rana, K., Shafer, M. M.,
739 Villalobos, A. M., and Schauer, J. J.: The Discoloration of the Taj Mahal due to Particulate
740 Carbon and Dust Deposition, *Environ. Sci. Technol.*, 49, 808-812, doi: 10.1021/es504005q,
741 2015.
- 742 Bisht, D. S., Dumka, U. C., Kaskaoutis, D. G., Pipal, A. S., Srivastava, A. K., Soni, V. K., Attri,
743 S. D., Sateesh, M., and Tiwari, S.: Carbonaceous aerosols and pollutants over Delhi urban
744 environment: Temporal evolution, source apportionment and radiative forcing, *Sci. Total*
745 *Environ.*, 521-522C, 431-445, doi: 10.1016/j.scitotenv.2015.03.083, 2015.
- 746 Bonasoni, P., Laj, P., Marinoni, A., Sprenger, M., Angelini, F., Arduini, J., Bonafè, U., Calzolari,
747 F., Colombo, T., Decesari, S., Di Biagio, C., di Sarra, A. G., Evangelisti, F., Duchi, R.,
748 Facchini, M. C., Fuzzi, S., Gobbi, G. P., Maione, M., Panday, A., Roccatò, F., Sellegri, K.,
749 Venzac, H., Verza, G. P., Villani, P., Vuillermoz, E., and Cristofanelli, P.: Atmospheric
750 Brown Clouds in the Himalayas: first two years of continuous observations at the Nepal
751 Climate Observatory-Pyramid (5079 m), *Atmospheric Chemistry and Physics*, 10, 7515-
752 7531, doi: 10.5194/acp-10-7515-2010, 2010.
- 753 Brimblecombe, P.: *The effects of air pollution on the built environment*, Imperial College Press,
754 London, 2003.
- 755 Burney, J., and Ramanathan, V.: Recent climate and air pollution impacts on Indian agriculture,
756 *Proc. Natl. Acad. Sci. USA*, 111, 16319-16324, doi: 10.1073/pnas.1317275111, 2014.
- 757 Cao, J.-J., Zhu, C.-S., Chow, J. C., Watson, J. G., Han, Y.-M., Wang, G.-h., Shen, Z.-x., and An,
758 Z.-S.: Black carbon relationships with emissions and meteorology in Xi'an, China,
759 *Atmospheric Research*, 94, 194-202, <http://dx.doi.org/10.1016/j.atmosres.2009.05.009>, 2009.
- 760 Cong, Z., Kang, S., Kawamura, K., Liu, B., Wan, X., Wang, Z., Gao, S., and Fu, P.:
761 Carbonaceous aerosols on the south edge of the Tibetan Plateau: concentrations, seasonality
762 and sources, *Atmospheric Chemistry and Physics*, 15, 1573-1584, doi: 10.5194/acp-15-
763 1573-2015, 2015a.
- 764 Cong, Z., Kawamura, K., Kang, S., and Fu, P.: Penetration of biomass-burning emissions from
765 South Asia through the Himalayas: new insights from atmospheric organic acids, *Scientific*
766 *Reports*, 5, 1-7, doi: 10.1038/srep09580, 2015b.
- 767 Cristofanelli, P., Bracci, A., Sprenger, M., Marinoni, A., Bonafè, U., Calzolari, F., Duchi, R.,
768 Laj, P., Pichon, J. M., Roccatò, F., Venzac, H., Vuillermoz, E., and Bonasoni, P.:
769 Tropospheric ozone variations at the Nepal Climate Observatory-Pyramid (Himalayas, 5079

770 m a.s.l.) and influence of deep stratospheric intrusion events, *Atmos. Chem. Phys.*, 10, 6537-
771 6549, doi: 10.5194/acp-10-6537-2010, 2010.

772 Das, S. K., and Jayaraman, A.: Role of black carbon in aerosol properties and radiative forcing
773 over western India during premonsoon period, *Atmos. Res.*, 102, 320-334, doi:
774 10.1016/j.atmosres.2011.08.003, 2011.

775 Day, D., Hand, J., Carrico, C., Engling, G., and Malm, W.: Humidification factors from
776 laboratory studies of fresh smoke from biomass fuels, *J. Geophys. Res.*, 111, D22202, doi:
777 10.1029/2006JD007221, 2006.

778 Dickerson, R. R., Andreae, M. O., Campos, T., Mayol-Bracero, O. L., Neusuess, C., and Streets,
779 D. G.: Analysis of black carbon and carbon monoxide observed over the Indian Ocean:
780 Implications for emissions and photochemistry, *Journal of Geophysical Research:*
781 *Atmospheres*, 107, INX2 16-11-INX12 16-11, 10.1029/2001JD000501, 2002.

782 Duchi, R., Cristofanelli, P., Marinoni, A., Laj, P., Marcq, S., Villani, P., Sellegri, K., Angelini,
783 F., Calzolari, F., Gobbi, G. P., Verza, G. P., Vuillermoz, E., Sapkota, A., and Bonasoni, P.:
784 Continuous observations of synoptic-scale dust transport at the Nepal Climate Observatory-
785 Pyramid (5079 m a.s.l.) in the Himalayas, *Atmos. Chem. Phys. Discuss.*, 11, 4229-4261, doi:
786 10.5194/acpd-11-4229-2011, 2011.

787 Forouzanfar, M. H., Alexander, L., Anderson, H. R., Bachman, V. F., Biryukov, S., Brauer, M.,
788 Burnett, R., Casey, D., Coates, M. M., and Cohen, A.: Global, regional, and national
789 comparative risk assessment of 79 behavioural, environmental and occupational, and
790 metabolic risks or clusters of risks in 188 countries, 1990–2013: a systematic analysis for the
791 Global Burden of Disease Study 2013, *Lancet*, 386, 2287-2323, doi: 10.1016/S0140-
792 6736(15)00128-2, 2015.

793 Ganguly, D., Jayaraman, A., Rajesh, T. A., and Gadhavi, H.: Wintertime aerosol properties
794 during foggy and nonfoggy days over urban center Delhi and their implications for
795 shortwave radiative forcing, *Journal of Geophysical Research*, 111, 1-15,
796 10.1029/2005jd007029, 2006.

797 Gaur, A., Tripathi, S. N., Kanawade, V. P., Tare, V., and Shukla, S. P.: Four-year measurements
798 of trace gases (SO₂, NO_x, CO, and O₃) at an urban location, Kanpur, in Northern India,
799 *Journal of Atmospheric Chemistry*, 71, 283-301, doi: 10.1007/s10874-014-9295-8, 2014.

800 Gauri, K. L., and Holdren, G.: Pollutant effects on stone monuments, *Environ. Sci. Technol.*, 15,
801 386-390, doi: 10.1021/es00086a001, 1981.

802 Girach, I. A., Nair, V. S., Babu, S. S., and Nair, P. R.: Black carbon and carbon monoxide over
803 Bay of Bengal during W_ICARB: Source characteristics, *Atmospheric Environment*, 94,
804 508-517, <http://dx.doi.org/10.1016/j.atmosenv.2014.05.054>, 2014.

805 Huang, X.-F., Sun, T.-L., Zeng, L.-W., Yu, G.-H., and Luan, S.-J.: Black carbon aerosol
806 characterization in a coastal city in South China using a single particle soot photometer,
807 *Atmospheric Environment*, 51, 21-28, 10.1016/j.atmosenv.2012.01.056, 2012.

808 IPCC: Climate Change 2013: The Physical Science Basis. Contribution of Working Group I to
809 the Fifth Assessment Report of the Intergovernmental Panel on Climate Change [Stocker,
810 T.F., D. Qin, G.-K. Plattner, M. Tignor, S.K. Allen, J. Boschung, A. Nauels, Y. Xia, V. Bex
811 and P.M. Midgley (eds.)]. , Cambridge University Press, Cambridge, United Kingdom and
812 New York, NY, USA, 1535 pp., 2013.

813 Jaffe, D., Mahura, A., Kelley, J., Atkins, J., Novelli, P. C., and Merrill, J.: Impact of Asian
814 emissions on the remote North Pacific atmosphere: Interpretation of CO data from Shemya,

815 Guam, Midway and Mauna Loa, *Journal of Geophysical Research*, 102, 28627,
816 10.1029/96jd02750, 1997.

817 Joshi, H., Naja, M., Singh, K., Kumar, R., Bhardwaj, P., Babu, S. S., Satheesh, S., Moorthy, K.
818 K., and Chandola, H.: Investigations of aerosol black carbon from a semi-urban site in the
819 Indo-Gangetic Plain region, *Atmos. Environ.*, 125, 346-359, doi:
820 10.1016/j.atmosenv.2015.04.007, 2016.

821 Kirchstetter, T. W., Novakov, T., and Hobbs, P. V.: Evidence that the spectral dependence of
822 light absorption by aerosols is affected by organic carbon, *Journal of Geophysical Research*,
823 109, 1-12, doi:10.1029/2004JD004999, 2004.

824 Kulkarni, S., Sobhani, N., Miller-Schulze, J. P., Shafer, M. M., Schauer, J. J., Solomon, P. A.,
825 Saide, P. E., Spak, S. N., Cheng, Y. F., Denier van der Gon, H. A. C., Lu, Z., Streets, D. G.,
826 Janssens-Maenhout, G., Wiedinmyer, C., Lantz, J., Artamonova, M., Chen, B., Imashev, S.,
827 Sverdlik, L., Deminter, J. T., Adhikary, B., D'Allura, A., Wei, C., and Carmichael, G. R.:
828 Source sector and region contributions to BC and PM_{2.5} in Central Asia, *Atmos. Chem.*
829 *Phys.*, 15, 1683-1705, doi: 10.5194/acp-15-1683-2015, 2015.

830 Kumar, B., Chakraborty, A., Tripathi, S. N., and Bhattu, D.: Highly time resolved chemical
831 characterization of submicron organic aerosols at a polluted urban location, *Environmental*
832 *Science: Processes & Impacts*, 18, 1285-1296, 10.1039/C6EM00392C, 2016a.

833 Kumar, M., Tiwari, S., Murari, V., Singh, A. K., and Banerjee, T.: Wintertime characteristics of
834 aerosols at middle Indo-Gangetic Plain: Impacts of regional meteorology and long range
835 transport, *Atmospheric Environment*, 104, 162-175, 10.1016/j.atmosenv.2015.01.014, 2015.

836 Kumar, V., Sarkar, C., and Sinha, V.: Influence of post harvest crop residue fires on surface
837 ozone mixing ratios in the NW IGP analyzed using two years of continuous in-situ trace gas
838 measurements, *J. Geophys. Res. Atmos.*, 121, 3619–3633, doi: 10.1002/2015JD024308,
839 2016b.

840 Lawrence, M. G., and Lelieveld, J.: Atmospheric pollutant outflow from southern Asia: a review,
841 *Atmos. Chem. Phys.*, 10, 11017-11096, doi: 10.5194/acp-10-11017-2010, 2010.

842 Lüthi, Z. L., Škerlak, B., Kim, S. W., Lauer, A., Mues, A., Rupakheti, M., and Kang, S.:
843 Atmospheric brown clouds reach the Tibetan Plateau by crossing the Himalayas,
844 *Atmospheric Chemistry and Physics*, 15, 6007-6021, 10.5194/acp-15-6007-2015, 2015.

845 Marinoni, A., Cristofanelli, P., Laj, P., Duchi, R., Putero, D., Calzolari, F., Landi, T. C.,
846 Vuillermoz, E., Maione, M., and Bonasoni, P.: High black carbon and ozone concentrations
847 during pollution transport in the Himalayas: Five years of continuous observations at NCO-P
848 global GAW station, *Journal of environmental Science* 25, 1618-1625, doi: 10.1016/s1001-
849 0742(12)60242-3, 2013.

850 Misra, A., Gaur, A., Bhattu, D., Ghosh, S., Dwivedi, A. K., Dalai, R., Paul, D., Gupta, T., Tare,
851 V., Mishra, S. K., Singh, S., and Tripathi, S. N.: An overview of the physico-chemical
852 characteristics of dust at Kanpur in the central Indo-Gangetic basin, *Atmospheric*
853 *Environment*, 97, 386-396, <http://dx.doi.org/10.1016/j.atmosenv.2014.08.043>, 2014.

854 Mohnen, V. A., Goldstein, W., and Wang, W. C.: Tropospheric Ozone and Climate Change, *Air*
855 *& Waste*, 43, 1332-1334, 10.1080/1073161x.1993.10467207, 1993.

856 Naja, M., Lal, S., and Chand, D.: Diurnal and seasonal variabilities in surface ozone at a high
857 altitude site Mt Abu (24.6° N, 72.7° E, 1680m asl) in India, *Atmos. Environ.*, 37, 4205-4215,
858 doi: 10.1016/S1352-2310(03)00565-X, 2003.

859 Naja, M., Mallik, C., Sarangi, T., Sheel, V., and Lal, S.: SO₂ measurements at a high altitude site
860 in the central Himalayas: Role of regional transport, *Atmos. Environ.*, 99, 392-402, doi:
861 10.1016/j.atmosenv.2014.08.031, 2014.

862 Pan, X. L., Kanaya, Y., Wang, Z. F., Liu, Y., Pochanart, P., Akimoto, H., Sun, Y. L., Dong, H.
863 B., Li, J., Irie, H., and Takigawa, M.: Correlation of black carbon aerosol and carbon
864 monoxide in the high-altitude environment of Mt. Huang in Eastern China, *Atmos. Chem.
865 Phys.*, 11, 9735-9747, doi: 10.5194/acp-11-9735-2011, 2011.

866 Panday, A. K., and Prinn, R. G.: Diurnal cycle of air pollution in the Kathmandu Valley, Nepal:
867 Observations, *Journal of Geophysical Research*, 114, 1-19, doi: 10.1029/2008jd009777,
868 2009.

869 Pathak, B., Bhuyan, P. K., Biswas, J., and Takemura, T.: Long term climatology of particulate
870 matter and associated microphysical and optical properties over Dibrugarh, North-East India
871 and inter-comparison with SPRINTARS simulations, *Atmospheric Environment*, 69, 334-
872 344, 10.1016/j.atmosenv.2012.12.032, 2013.

873 Praveen, P. S., Ahmed, T., Kar, A., Rehman, I. H., and Ramanathan, V.: Link between local
874 scale BC emissions in the Indo-Gangetic Plains and large scale atmospheric solar absorption,
875 *Atmospheric Chemistry and Physics*, 12, 1173-1187, 10.5194/acp-12-1173-2012, 2012.

876 Putero, D., Landi, T., Cristofanelli, P., Marinoni, A., Laj, P., Duchi, R., Calzolari, F., Verza, G.,
877 and Bonasoni, P.: Influence of open vegetation fires on black carbon and ozone variability in
878 the southern Himalayas (NCO-P, 5079 m asl), *Environmental Pollution*, 184, 597-604,
879 10.1016/j.envpol.2013.09.035, 2014.

880 Putero, D., Cristofanelli, P., Marinoni, A., Adhikary, B., Duchi, R., Shrestha, S. D., Verza, G. P.,
881 Landi, T. C., Calzolari, F., Busetto, M., Agrillo, G., Biancofiore, F., Di Carlo, P., Panday, A.
882 K., Rupakheti, M., and Bonasoni, P.: Seasonal variation of ozone and black carbon observed
883 at Paknajol, an urban site in the Kathmandu Valley, Nepal, *Atmos. Chem. Phys.*, 15, 13957-
884 13971, doi: 10.5194/acp-15-13957-2015, 2015.

885 Ram, K., Sarin, M., and Tripathi, S.: A 1 year record of carbonaceous aerosols from an urban site
886 in the Indo-Gangetic Plain: Characterization, sources, and temporal variability, *J. Geophys.
887 Res.*, 115, D24313, doi: 10.1029/2010JD014188, 2010.

888 Ramachandran, S., and Rajesh, T. A.: Black carbon aerosol mass concentrations over
889 Ahmedabad, an urban location in western India: Comparison with urban sites in Asia,
890 Europe, Canada, and the United States, *Journal of Geophysical Research: Atmospheres*, 112,
891 n/a-n/a, 10.1029/2006JD007488, 2007.

892 Ramanathan, V., Li, F., Ramana, M., Praveen, P., Kim, D., Corrigan, C., Nguyen, H., Stone, E.
893 A., Schauer, J. J., and Carmichael, G.: Atmospheric brown clouds: Hemispherical and
894 regional variations in long-range transport, absorption, and radiative forcing, *J. Geophys.
895 Res.*, 112, D22S21, doi: 10.1029/2006JD008124, 2007.

896 Ramanathan, V., and Carmichael, G.: Global and regional climate changes due to black carbon,
897 *Nat. Geosci.*, 1, 221-227, 2008.

898 Rastogi, N., Singh, A., Sarin, M. M., and Singh, D.: Temporal variability of primary and
899 secondary aerosols over northern India: Impact of biomass burning emissions, *Atmos.
900 Environ.*, 125, 396-403, doi: 10.1016/j.atmosenv.2015.06.010, 2016.

901 Rehman, I. H., Ahmed, T., Praveen, P. S., Kar, A., and Ramanathan, V.: Black carbon emissions
902 from biomass and fossil fuels in rural India, *Atmospheric Chemistry and Physics*, 11, 7289-
903 7299, 10.5194/acp-11-7289-2011, 2011.

904 Safai, P. D., Kewat, S., Pandithurai, G., Praveen, P. S., Ali, K., Tiwari, S., Rao, P. S. P.,
905 Budhawant, K. B., Saha, S. K., and Devara, P. C. S.: Aerosol characteristics during winter
906 fog at Agra, North India, *J. Atmos. Chem.*, 61, 101-118, doi: 10.1007/s10874-009-9127-4,
907 2009.

908 Sandradewi, J., Prévôt, A. S. H., Szidat, S., Perron, N., Alfarra, M. R., Lanz, V. A., Weingartner,
909 E., and Baltensperger, U.: Using Aerosol Light Absorption Measurements for the
910 Quantitative Determination of Wood Burning and Traffic Emission Contributions to
911 Particulate Matter, *Environmental Science & Technology*, 42, 3316-3323, doi:
912 10.1021/es702253m, 2008.

913 Sarkar, C., Kumar, V., and Sinha, V.: Massive emissions of carcinogenic benzenoids from paddy
914 residue burning in north India, *Curr. Sci. India*, 104, 1703-1709, 2013.

915 Schmid, O., Artaxo, P., Arnott, W. P., Chand, D., Gatti, L. V., Frank, G. P., Hoffer, A.,
916 Schnaiter, M., and Andreae, M. O.: Spectral light absorption by ambient aerosols influenced
917 by biomass burning in the Amazon Basin. I: Comparison and field calibration of absorption
918 measurement techniques, *Atmospheric Chemistry and Physics*, 6, 3443-3462, doi:
919 10.5194/acp-6-3443-2006, 2006.

920 Sharma, R. K., Bhattarai, B. K., Sapkota, B. K., Gewali, M. B., and Kjeldstad, B.: Black carbon
921 aerosols variation in Kathmandu valley, Nepal, *Atmos. Environ.*, 63, 282-288,
922 10.1016/j.atmosenv.2012.09.023, 2012.

923 Sharma, S., Brook, J. R., Cachier, H., Chow, J., Gaudenzi, A., and Lu, G.: Light absorption and
924 thermal measurements of black carbon in different regions of Canada, *Journal of
925 Geophysical Research: Atmospheres*, 107, AAC 11-11-AAC 11-11, 10.1029/2002JD002496,
926 2002.

927 Shindell, D.: Integrated Assessment of Black Carbon and Tropospheric Ozone: Summary for
928 Decision Makers, United Nations Environment Programme, 303pp., 2011.

929 Singh, N., Murari, V., Kumar, M., Barman, S. C., and Banerjee, T.: Fine particulates over South
930 Asia: Review and meta-analysis of PM_{2.5} source apportionment through receptor model,
931 *Environmental Pollution*, 223, 121-136, 10.1016/j.envpol.2016.12.071, 2017.

932 Sinha, V., Kumar, V., and Sarkar, C.: Chemical composition of pre-monsoon air in the Indo-
933 Gangetic Plain measured using a new air quality facility and PTR-MS: high surface ozone
934 and strong influence of biomass burning, *Atmospheric Chemistry and Physics*, 14, 5921-
935 5941, 10.5194/acp-14-5921-2014, 2014.

936 Skamarock, W., Klemp, J., Dudhia, J., Gill, D., and Barker, D.: A description of the Advanced
937 Research WRF version 3, Technical Report NCAR/TN475+STR, National Center for
938 Atmospheric Research Technical Note, Boulder, Colorado, 2008.

939 Snider, G., Weagle, C. L., Murdymootoo, K. K., Ring, A., Ritchie, Y., Stone, E., Walsh, A.,
940 Akoshile, C., Anh, N. X., Balasubramanian, R., Brook, J., Qonitan, F. D., Dong, J., Griffith,
941 D., He, K., Holben, B. N., Kahn, R., Lagrosas, N., Lestari, P., Ma, Z., Misra, A., Norford, L.
942 K., Quel, E. J., Salam, A., Schichtel, B., Segev, L., Tripathi, S., Wang, C., Yu, C., Zhang, Q.,
943 Zhang, Y., Brauer, M., Cohen, A., Gibson, M. D., Liu, Y., Martins, J. V., Rudich, Y., and
944 Martin, R. V.: Variation in global chemical composition of PM_{2.5}: emerging results from
945 SPARTAN, *Atmos. Chem. Phys.*, 16, 9629-9653, 10.5194/acp-16-9629-2016, 2016.

946 Srivastava, A. K., Tiwari, S., Devara, P. C. S., Bisht, D. S., Srivastava, M. K., Tripathi, S. N.,
947 Goloub, P., and Holben, B. N.: Pre-monsoon aerosol characteristics over the Indo-Gangetic

948 Basin: implications to climatic impact, *Annales Geophysicae*, 29, 789-804, doi:
949 10.5194/angeo-29-789-2011, 2011.

950 Stevenson, D., Dentener, F., Schultz, M., Ellingsen, K., Van Noije, T., Wild, O., Zeng, G.,
951 Amann, M., Atherton, C., and Bell, N.: Multimodel ensemble simulations of present-day and
952 near-future tropospheric ozone, *J. Geophys. Res.*, 111, D08301, doi: 10.1029/2005JD006338,
953 2006.

954 Tiwari, S., Srivastava, A. K., Bisht, D. S., Parmita, P., Srivastava, M. K., and Attri, S. D.:
955 Diurnal and seasonal variations of black carbon and PM_{2.5} over New Delhi, India: Influence
956 of meteorology, *Atmospheric Research*, 125-126, 50-62, 10.1016/j.atmosres.2013.01.011,
957 2013.

958 Tiwari, S., Pipal, A. S., Hopke, P. K., Bisht, D. S., Srivastava, A. K., Tiwari, S., Saxena, P. N.,
959 Khan, A. H., and Pervez, S.: Study of the carbonaceous aerosol and morphological analysis
960 of fine particles along with their mixing state in Delhi, India: a case study, *Environmental
961 Science and Pollution Research*, 22, 10744-10757, 10.1007/s11356-015-4272-6, 2015.

962 Tiwari, S., Dumka, U. C., Kaskaoutis, D. G., Ram, K., Panicker, A. S., Srivastava, M. K.,
963 Tiwari, S., Attri, S. D., Soni, V. K., and Pandey, A. K.: Aerosol chemical characterization
964 and role of carbonaceous aerosol on radiative effect over Varanasi in central Indo-Gangetic
965 Plain, *Atmospheric Environment*, 125, 437-449, 10.1016/j.atmosenv.2015.07.031, 2016.

966 Tiwari, S., Dumka, U. C., Gautam, A. S., Kaskaoutis, D. G., Srivastava, A. K., Bisht, D. S.,
967 Chakrabarty, R. K., Sumlin, B. J., and Solmon, F.: Assessment of PM_{2.5} and PM₁₀ over
968 Guwahati in Brahmaputra River Valley: Temporal evolution, source apportionment and
969 meteorological dependence, *Atmospheric Pollution Research*, 8, 13-28,
970 10.1016/j.apr.2016.07.008, 2017.

971 Trivedi, D. K., Ali, K., and Beig, G.: Impact of meteorological parameters on the development of
972 fine and coarse particles over Delhi, *Science of The Total Environment*, 478, 175-183,
973 10.1016/j.scitotenv.2014.01.101, 2014.

974 Verma, R. L., Sahu, L. K., Kondo, Y., Takegawa, N., Han, S., Jung, J. S., Kim, Y. J., Fan, S.,
975 Sugimoto, N., Shammaa, M. H., Zhang, Y. H., and Zhao, Y.: Temporal variations of black
976 carbon in Guangzhou, China, in summer 2006, *Atmos. Chem. Phys.*, 10, 6471-6485, doi:
977 10.5194/acp-10-6471-2010, 2010.

978 Wan, X., Kang, S., Li, Q., Rupakheti, D., Zhang, Q., Guo, J., Chen, P., Tripathee, L., Rupakheti,
979 M., Panday, A. K., Wang, W., Kawamura, K., Gao, S., Wu, G., and Cong, Z.: Organic
980 molecular tracers in the atmospheric aerosols from Lumbini, Nepal, in the northern Indo-
981 Gangetic Plain: Influence of biomass burning, *Atmos. Chem. Phys. Discuss.*, 2017, 1-40,
982 10.5194/acp-2016-1176, 2017.

983 WHO: Air quality guidelines: global update 2005: particulate matter, ozone, nitrogen dioxide,
984 and sulfur dioxide, World Health Organization, Geneva, 22 pp., 2006.

985 Wiedinmyer, C., Akagi, S. K., Yokelson, R. J., Emmons, L. K., Al-Saadi, J. A., Orlando, J. J.,
986 and Soja, A. J.: The Fire INventory from NCAR (FINN): a high resolution global model to
987 estimate the emissions from open burning, *Geosci. Model Dev.*, 4, 625-641, doi:
988 10.5194/gmd-4-625-2011, 2011.

989 Zhou, X., Gao, J., Wang, T., Wu, W., and Wang, W.: Measurement of black carbon aerosols near
990 two Chinese megacities and the implications for improving emission inventories,
991 *Atmospheric Environment*, 43, 3918-3924, 10.1016/j.atmosenv.2009.04.062, 2009.

992

993 **Table 1.** Summary of instruments deployed during monitoring in Lumbini

Instrument (Model)	Manufacturer	Parameters	Inlet/sensor height (above ground)	Sampling interval	Sampled period
Environmental Dust monitor (EDM 164)	GRIMM Aerosol Technik, Germany	PM ₁ , PM _{2.5} , PM ₁₀	5 m	5 min	04/02-05/10, 06/02-06/13
Aethalometer (AE42)	Magee Scientific, USA	Aerosol light absorption at seven wavelengths, and BC concentration	3 m	5 min	01/04-05/06
CO analyzer (48i)	Thermo Scientific, USA	CO concentration	3 m	1 min	01/04-15/06
O ₃ analyzer (49i)	Thermo Scientific, USA	O ₃ concentration	3 m	1 min	01/04-15/06
Automatic Weather Station (AWS)	Campbell Scientific, UK	T, RH, WS, WD, Global Radiation, Precipitation	12 m	1 min	01/04-15/06

994

995

996 **Table 2.** Comparison of PM_{2.5}, BC, CO and O₃ concentrations at Lumbini with those at other sites in South Asia

Sites	Characteristics	Measurement period	PM _{2.5} (µg m ⁻³)	BC (µg/m ³)	CO (ppbv)	O ₃ (ppbv)	References
Lumbini, Nepal	Semi-urban	Pre-monsoon, 2013	53.1±35.1	4.9±3.8	344.1±160.3	46.6±20.3	This study
Kathmandu, Nepal	Urban	Pre-monsoon, 2013	-	14.5±10	-	38.0±25.6	(Putero et al., 2015)
Mt. Everest, Nepal	Remote	Pre-monsoon	-	0.4±0.4	-	61.3±7.7	(Marinoni et al., 2013)
Delhi, India	Urban	Pre-monsoon (night-time)	82.3±50.5	7.70±7.25	1800±890	-	(Bisht et al., 2015)
Kanpur, India	Urban	June 2009-May 2013, April-June	-	2.1±0.9	721±403	27.9±17.8	(Gaur et al., 2014) (Ram et al., 2010)
Mohali, India	Semi-urban	May, 2012	104±80.3	-	566.7±239.2	57.8±25.4	(Sinha et al., 2014)
Mt. Abu, India	Remote	Jan 1993-Dec 2000, pre-monsoon	-	0.7±0.14	131±36	39.9±10.8	(Naja et al., 2003) (Das and Jayaraman, 2011)

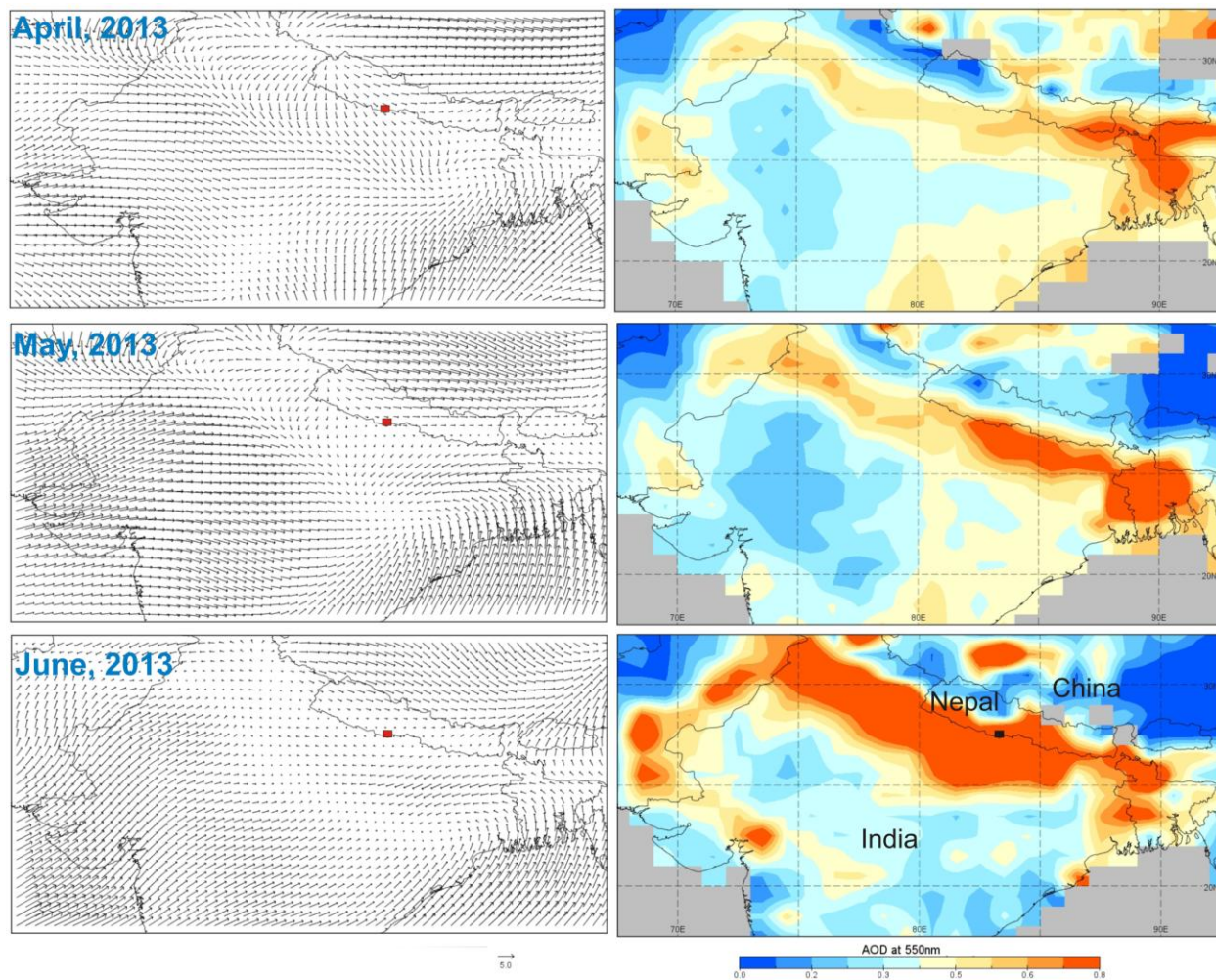
997 **Table 3.** Inter-comparison of observed and model simulated hourly average concentrations of air
998 pollutants during the measurement campaign period. Unit: BC and PM in $\mu\text{g}/\text{m}^3$ and CO in ppbv.

Pollutants	Observed (mean and range)	Modeled (mean and range)	Ratio of mean (observed/modeled)
BC	4.9 (0.3-29.9)	1.8 (0.4-3.7)	2.7
PM₁	36.6 (3.6-197.6)	12.3 (0.9-41.7)	3
PM_{2.5}	53.1 (6.1-272.2)	17.3 (1.9-48.3)	3
PM₁₀	128.8 (10.5-604.0)	25.4 (2.1-68.8)	5
CO	344.1(124.9-1429.7)	255.7 (72.2-613.1)	1.35

999

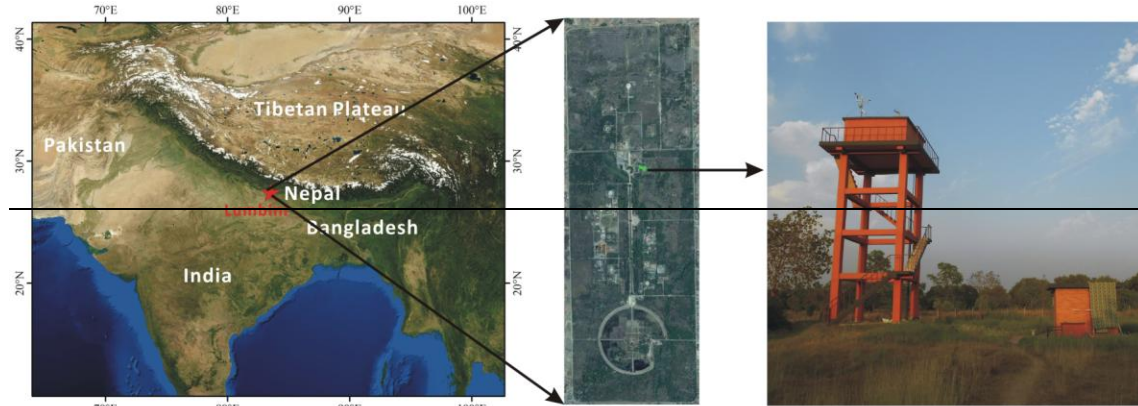
1000

1001 **Figures**



1002
1003 **Figure 1.** Monthly synoptic wind (at 1000 hPa) for April, May and June 2013, based on
1004 NCEP/NCAR reanalysis data where the orientations of arrows refer to wind direction and the
1005 length of arrows represents the magnitude of wind (m/s). Red square box in the figure (left)
1006 represents the location of Lumbini. Figures on the right side represent monthly aerosol optical
1007 depth acquired with the MODIS instrument aboard TERRA satellite. High aerosol loading can be
1008 seen over the entire Ingo-Gangetic Plains (IGP). Light gray color used in the figure represents
1009 the absence of data.

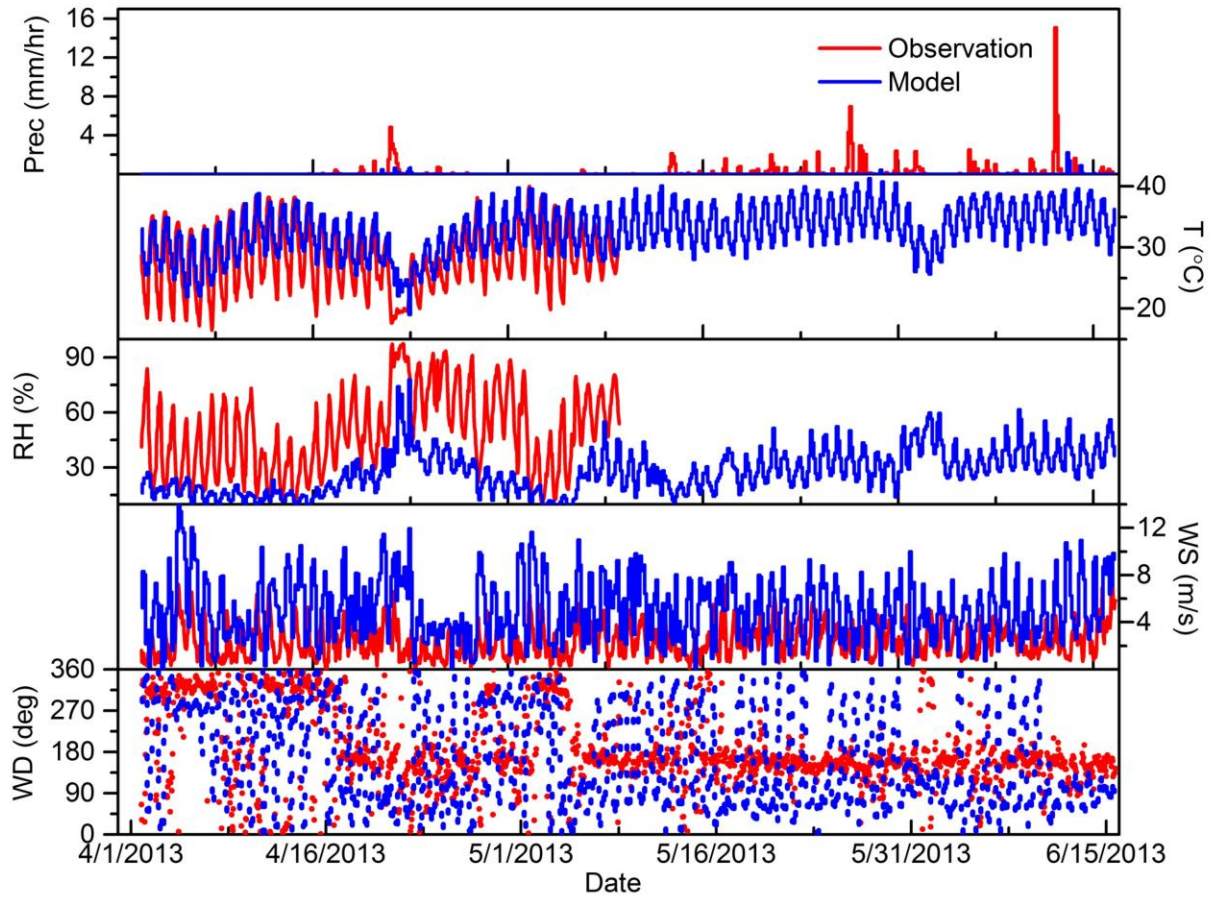
1010



1011
1012 **Figure 2.** Location of sampling site in Lumbini in southern Nepal (left panel). The middle panel
1013 shows the Kenzo Tange Master Plan Area of Lumbini while the right panel shows the sampling
1014 tower in the Lumbini Master Plan Area.

1015

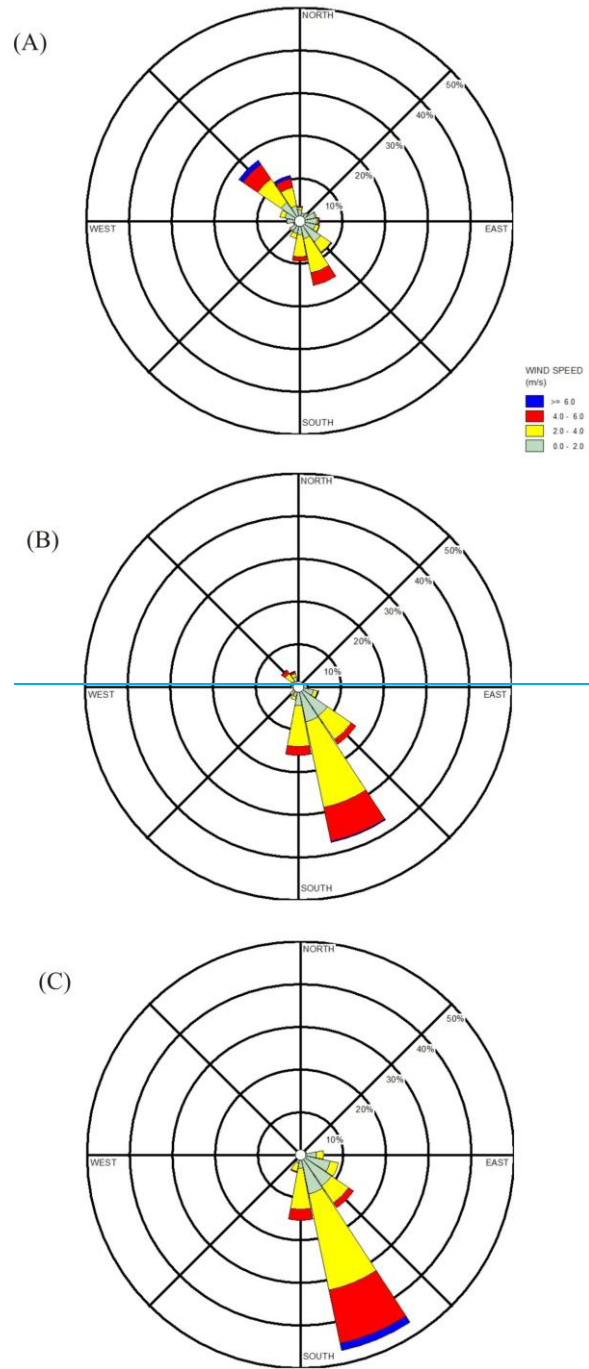
1016



1017

1018 **Figure 2.** Time series of hourly average observed (red) and model estimated (blue)
 1019 meteorological parameters at Lumbini, Nepal for the entire sampling period from 1 April to 15
 1020 June 2013.

1021



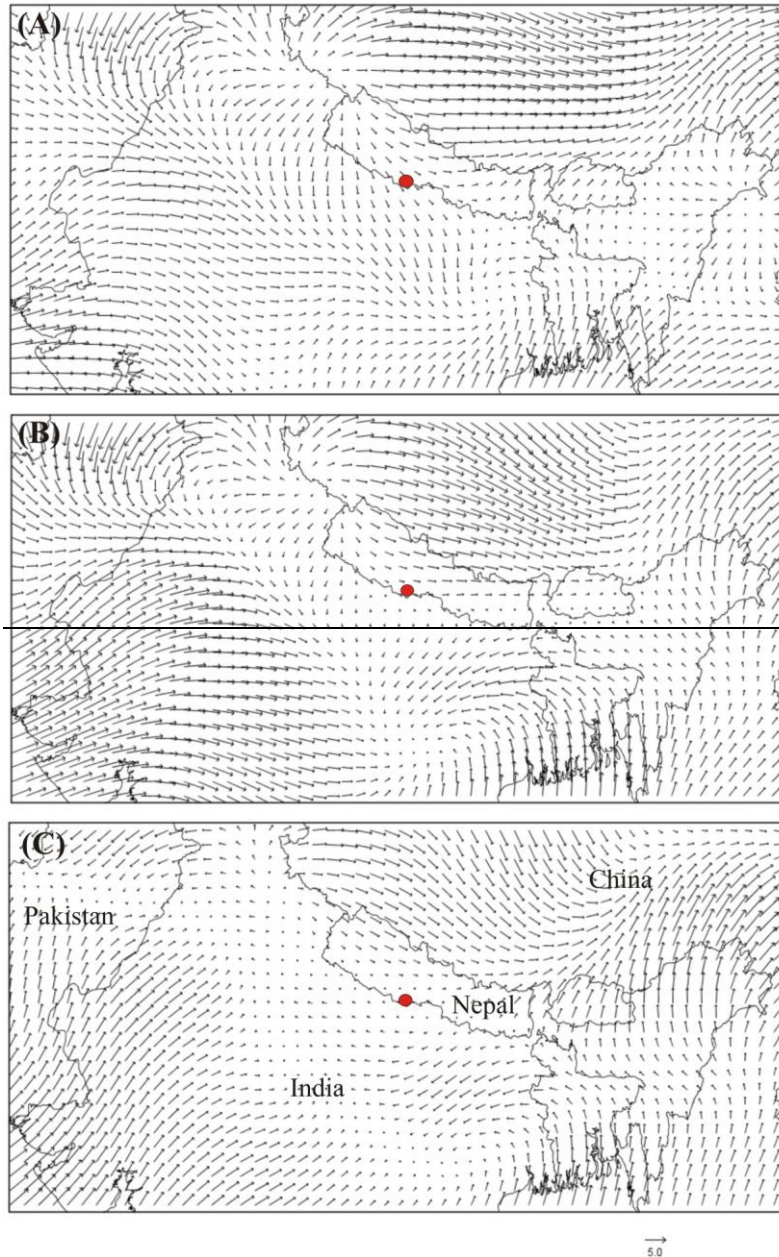
1022

1023 **Figure 4.** Wind rose of wind speed and wind direction observed at Lumbini during the month of

1024 (A) April, (B) May, and (C) (1st-15th) June 2013.

1025

1026



1027

1028 **Figure 5.** Monthly synoptic surface winds for the month of (A) April, (B) May and (C) June

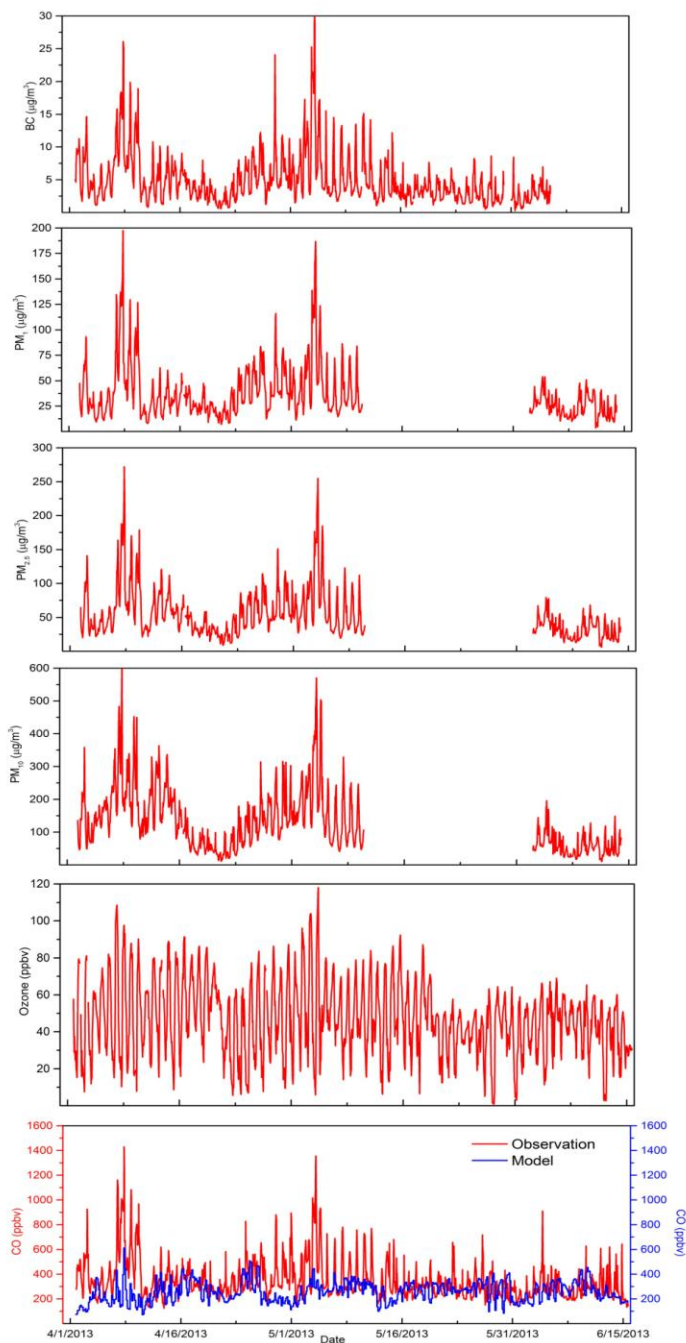
1029 2013, based on NCEP/NCAR reanalysis data. Orientations of arrows in the figures refer to wind

1030 direction whereas the length of arrows represents the magnitude of wind speed (m/s). Red dot in

1031 the map represents the location of Lumbini.

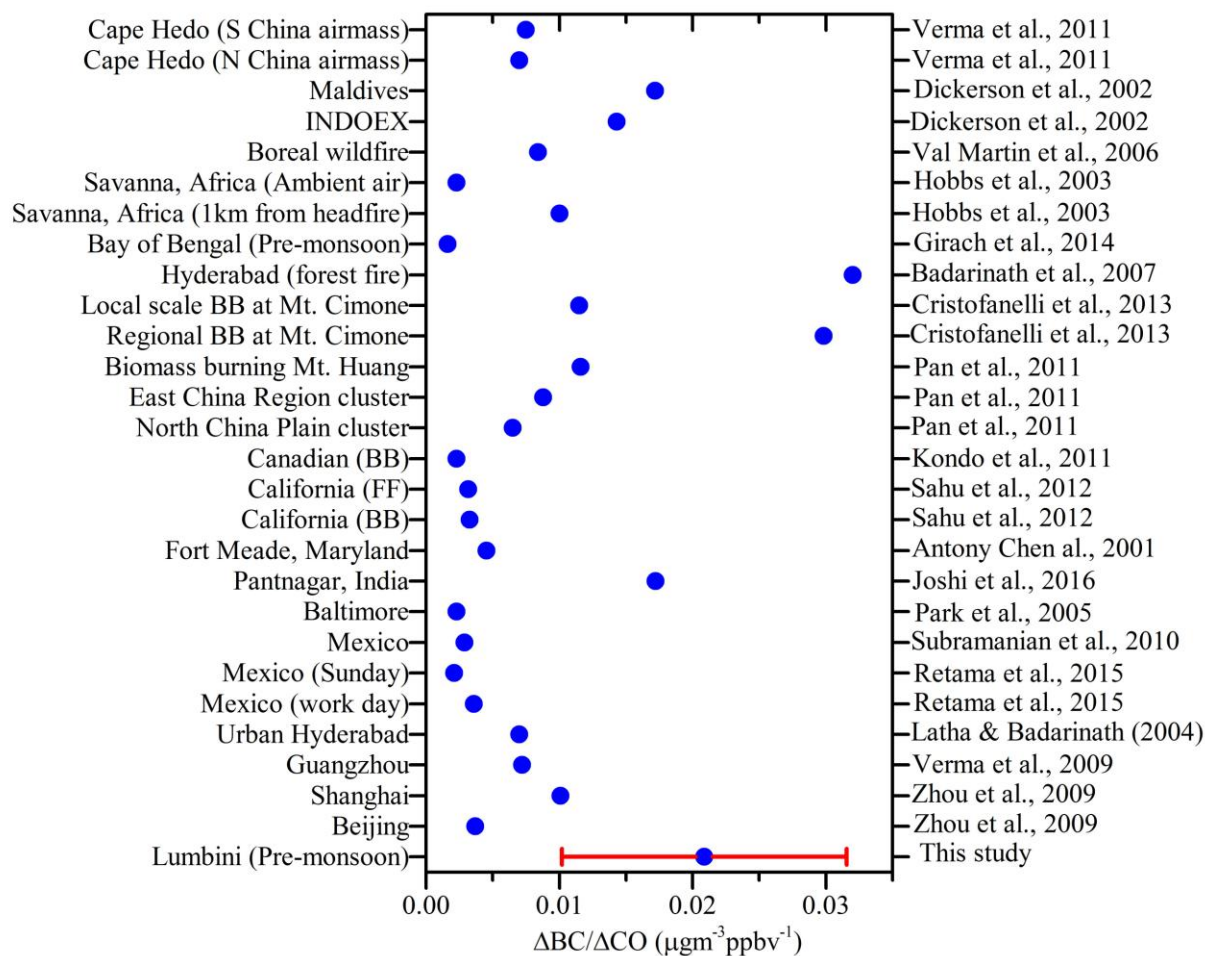
1032

1033



1035

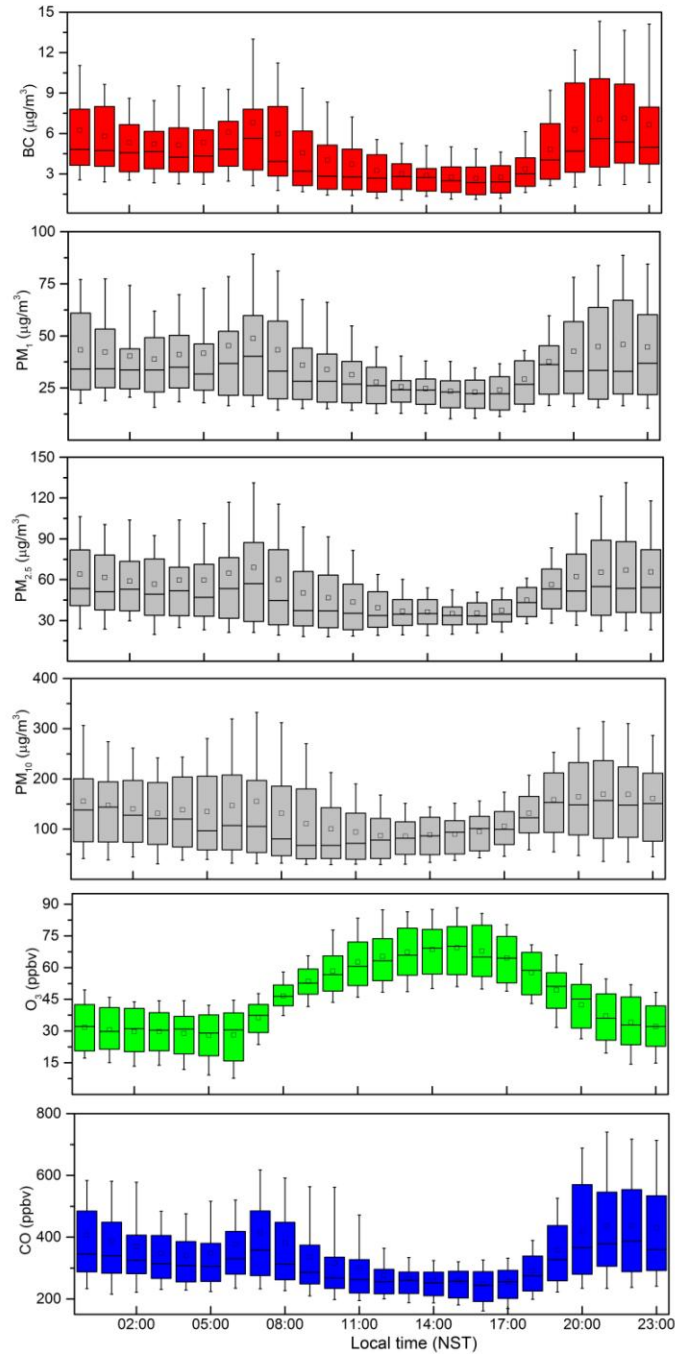
1036 **Figure 3.** Time series of the observed (red line) and model estimated (blue line) hourly average
 1037 concentrations of BC, PM₁, PM_{2.5}, PM₁₀, O₃ and CO at Lumbini, Nepal for the entire sampling
 1038 period from 1 April to 15 June 2013.



1040

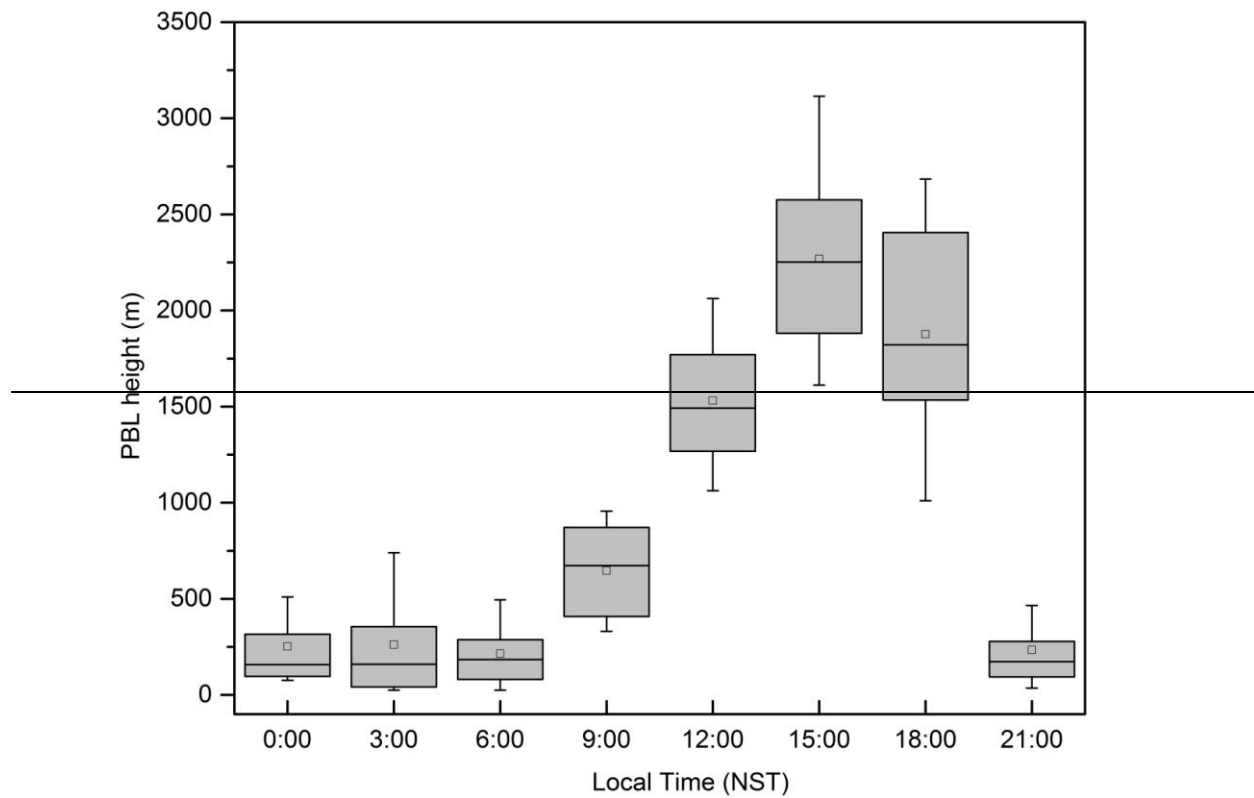
1041 **Figure 4.** Comparison of BC concentrations to CO concentrations ($\Delta BC/\Delta CO$) ratios obtained
 1042 for Lumbini with other sites. The red horizontal bar represents standard deviation.

1043



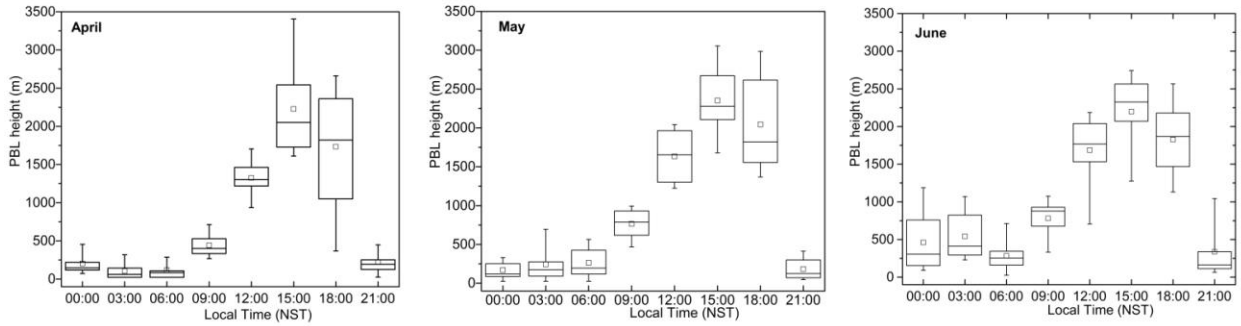
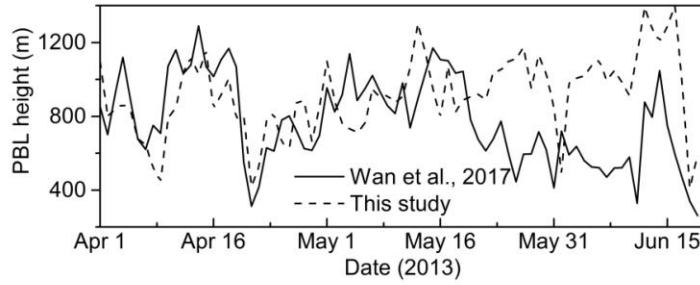
1044

1045 **Figure 5.** Diurnal variations of hourly average ambient concentrations of BC, PM₁, PM_{2.5}, PM₁₀,
 1046 O₃ and CO at Lumbini during the monitoring period (1 April -15 June 2013). In each box, lower
 1047 and upper boundary of the box represents 25th and 75th percentile respectively, top and bottom of
 1048 the whisker represents 90th and 10th percentile respectively, the mid-line represents median, and
 1049 the square mark represents the mean for each hour.



1050

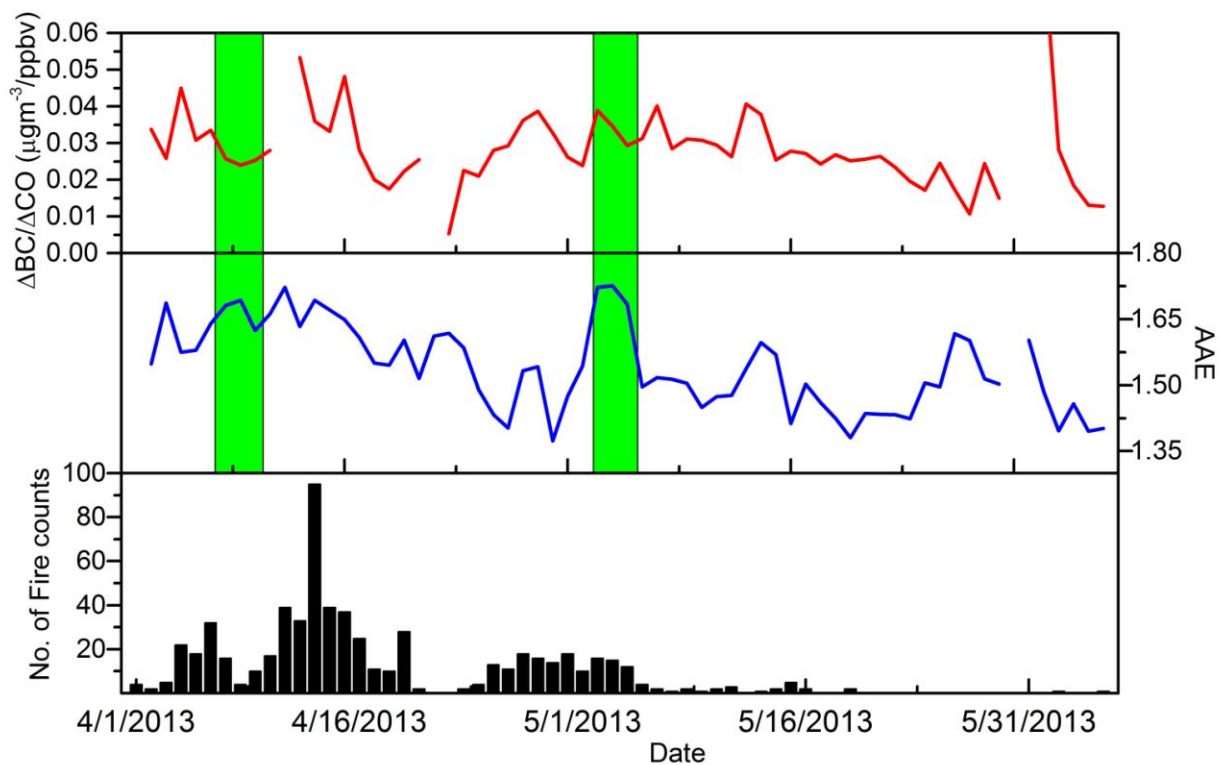
1051 **Figure 9.** Diurnal variation of the planetary boundary layer (PBL) height at Lumbini obtained
 1052 for every three hours of each day from the WRF STEM model for the sampling period. The
 1053 square mark in each box represents the mean PBL height, bottom and top of the box represents
 1054 25th and 75th percentile, top and bottom of the whisker represents 90th and 10th percentile
 1055 respectively.



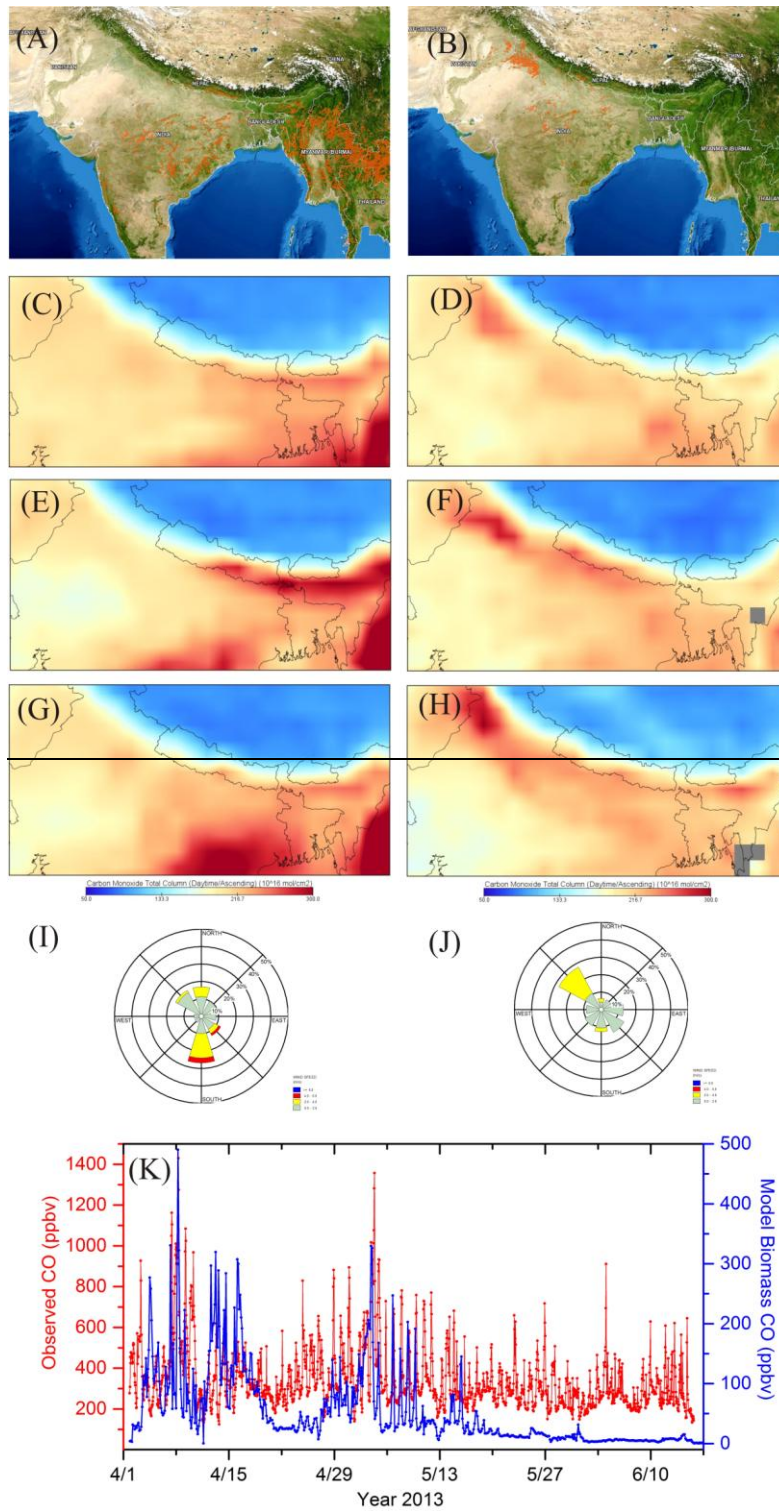
1056

1057 **Figure 6.** Daily time series of PBL height obtained from the model and reported values over
 1058 **Lumbini** (obtained from Xin et al., 2017). The lower panel shows the monthly average diurnal
 1059 variation of the PBL height. The square mark in each box represents the mean PBL height,
 1060 bottom and top of the box represents 25th and 75th percentile, top and bottom of the whisker
 1061 represents 90th and 10th percentile respectively.

1062



1063
 1064 Figure 7. Time series of daily average $\Delta BC/\Delta CO$ ratio, absorption Ångstrom exponent (AAE),
 1065 along with fire counts acquired with the MODIS instrument onboard TERRA satellite for a
 1066 200×200 km grid centered at Lumbini. Two rectangular green boxes represent time of two
 1067 episodes with high peaks in CO and BC concentrations as shown in earlier figures.
 1068

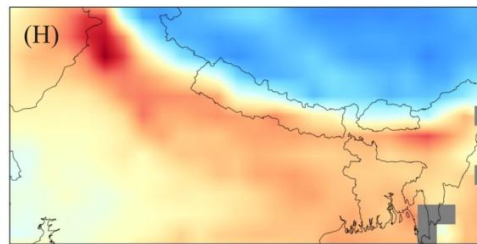
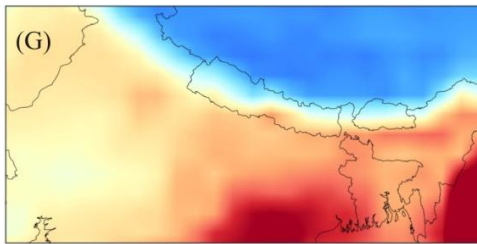
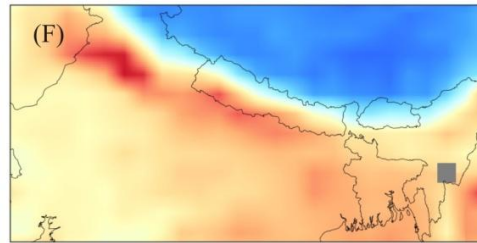
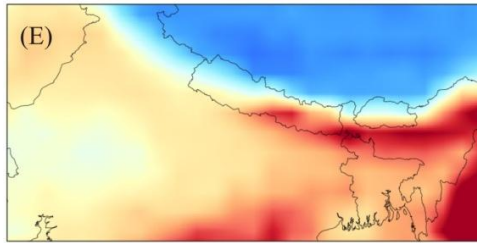
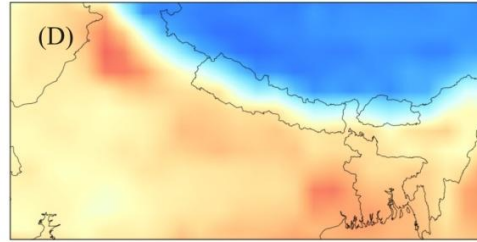
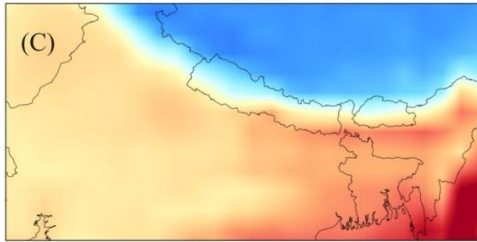
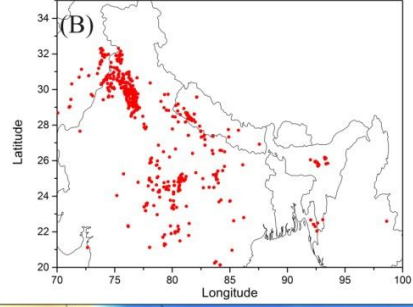
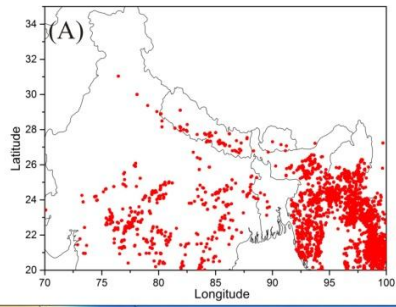


1069

1070 ~~Figure 9. Active fire hotspots in the region acquired with the MODIS instrument on Aqua~~

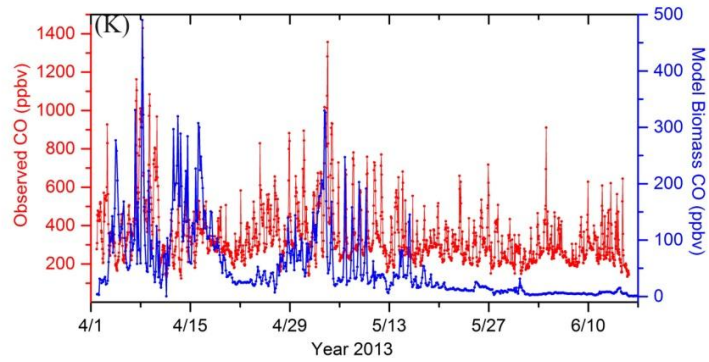
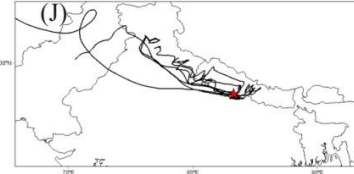
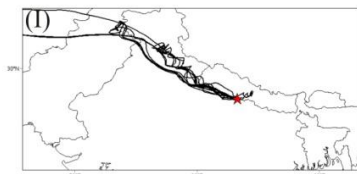
1071 ~~satellite during (A) Event I (7-9 April) and (B) Event II (3-4 May). CO emissions, acquired with~~

1072 ~~AIRS satellite, in the region two days before (3-5 April), during (7-9 April) and two days after~~
1073 ~~(10-12 April) the Event I are shown in panels (C), (E) and (G), respectively while panels (D), (F)~~
1074 ~~and (H) show CO emissions two days before (1-2 May), during (3-4 May) and two days after (5-~~
1075 ~~6 May) the Event II. Panels (I) and (J) represent the 6-hr interval HYSPLIT back trajectories~~
1076 ~~during Event I and II, respectively. Location of the Lumbini site is indicated by the red star in the~~
1077 ~~panel (I and J). Observed CO versus Model open burning CO illustrating the contribution of~~
1078 ~~forest fires during peak CO loading is shown in panel (K).~~



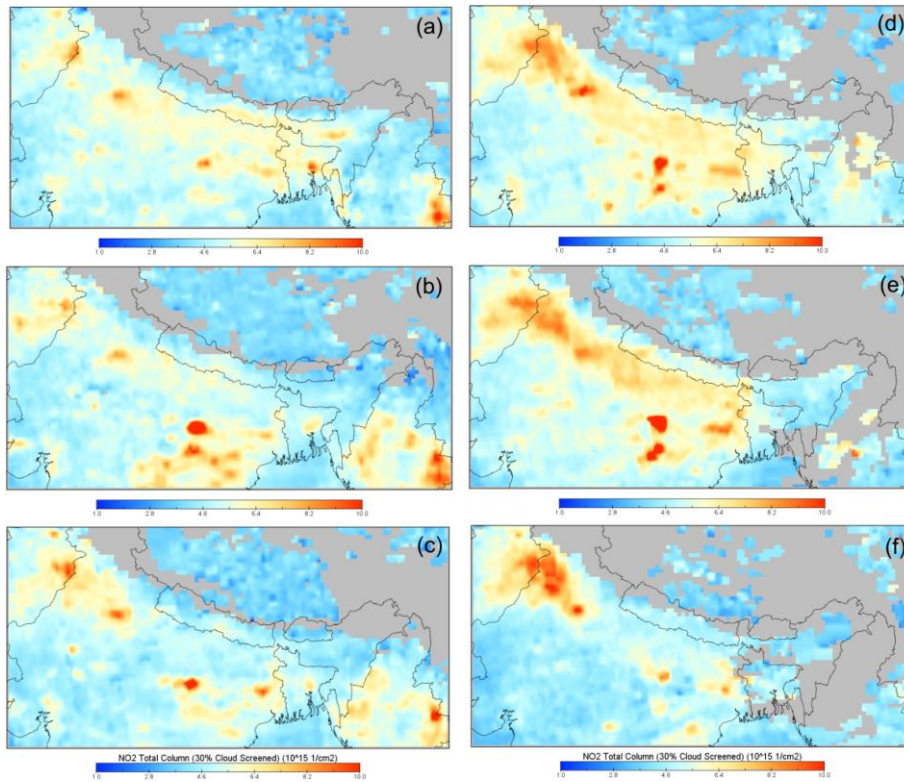
Carbon Monoxide Total Column (Daytime/Ascending) (10^{16} mol/cm²)

Carbon Monoxide Total Column (Daytime/Ascending) (10^{16} mol/cm²)



1080 Figure 8. Active fire hotspots in the region acquired with the MODIS instrument on Aqua
1081 satellite during (A) Event-I (7-9 April) and (B) Event-II (3-4 May). CO emissions, acquired with
1082 AIRS satellite, in the region two days before (3-5 April), during (7-9 April) and two days after
1083 (10-12 April) the Event-I are shown in panels (C), (E) and (G), respectively while panels (D), (F)
1084 and (H) show CO emissions two days before (1-2 May), during (3-4 May) and two days after (5-
1085 6 May) the Event-II. **Panels (I) and (J) represent the 6-hr interval HYSPLIT back trajectories**
1086 **during Event I and II, respectively.** Location of the Lumbini site is indicated by the red star in the
1087 panel (I and J). Observed CO versus Model open burning CO illustrating the contribution of
1088 forest fires during peak CO loading is shown in panel (K).

1089

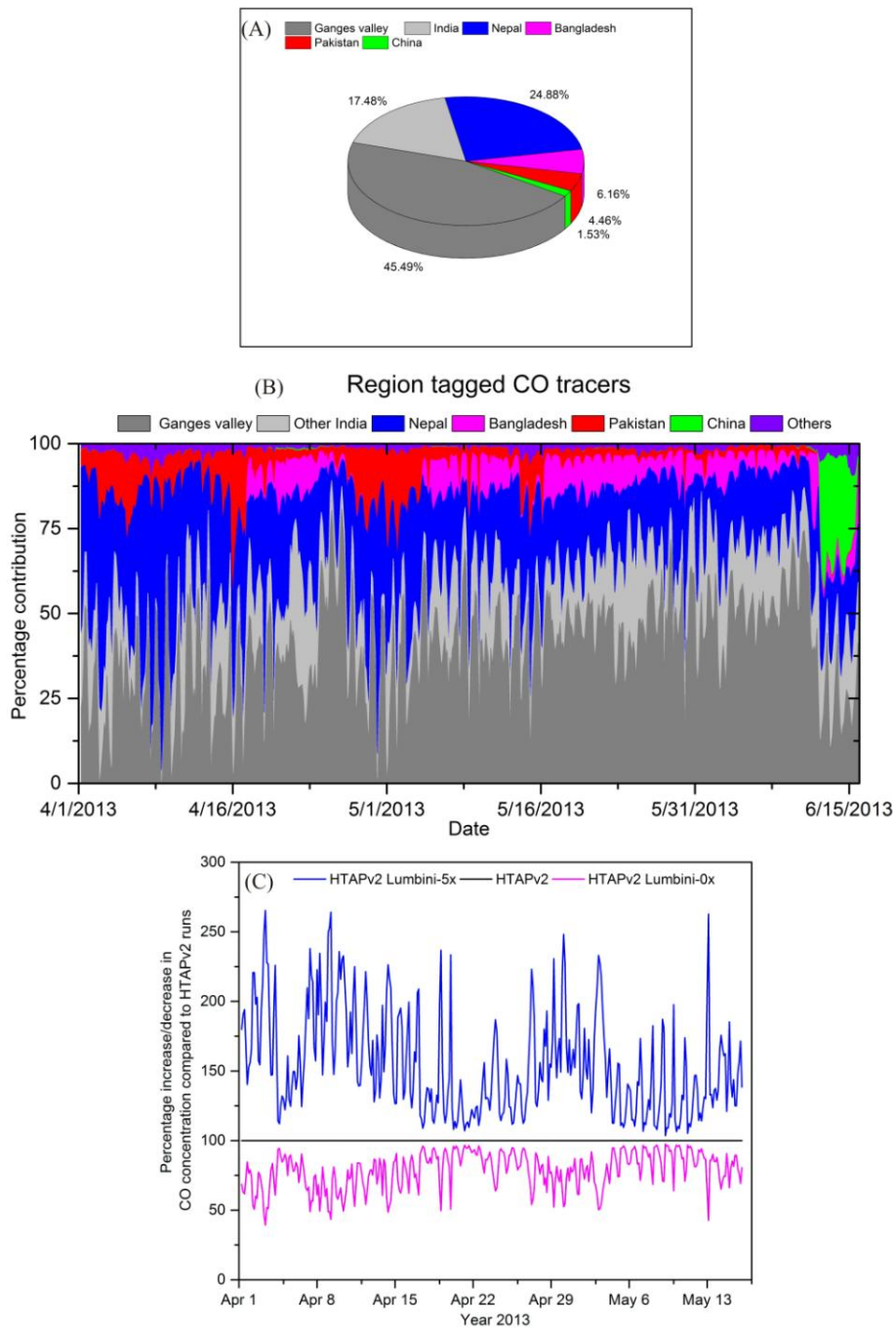


1090

1091 **Figure 9.** NO₂ total column obtained with OMI satellite over the region (a) before, (b) during,
 1092 and (c) after the Event- I. The panels (d), (e), (f) show NO₂ total column before, during and after
 1093 the Event- II.

1094

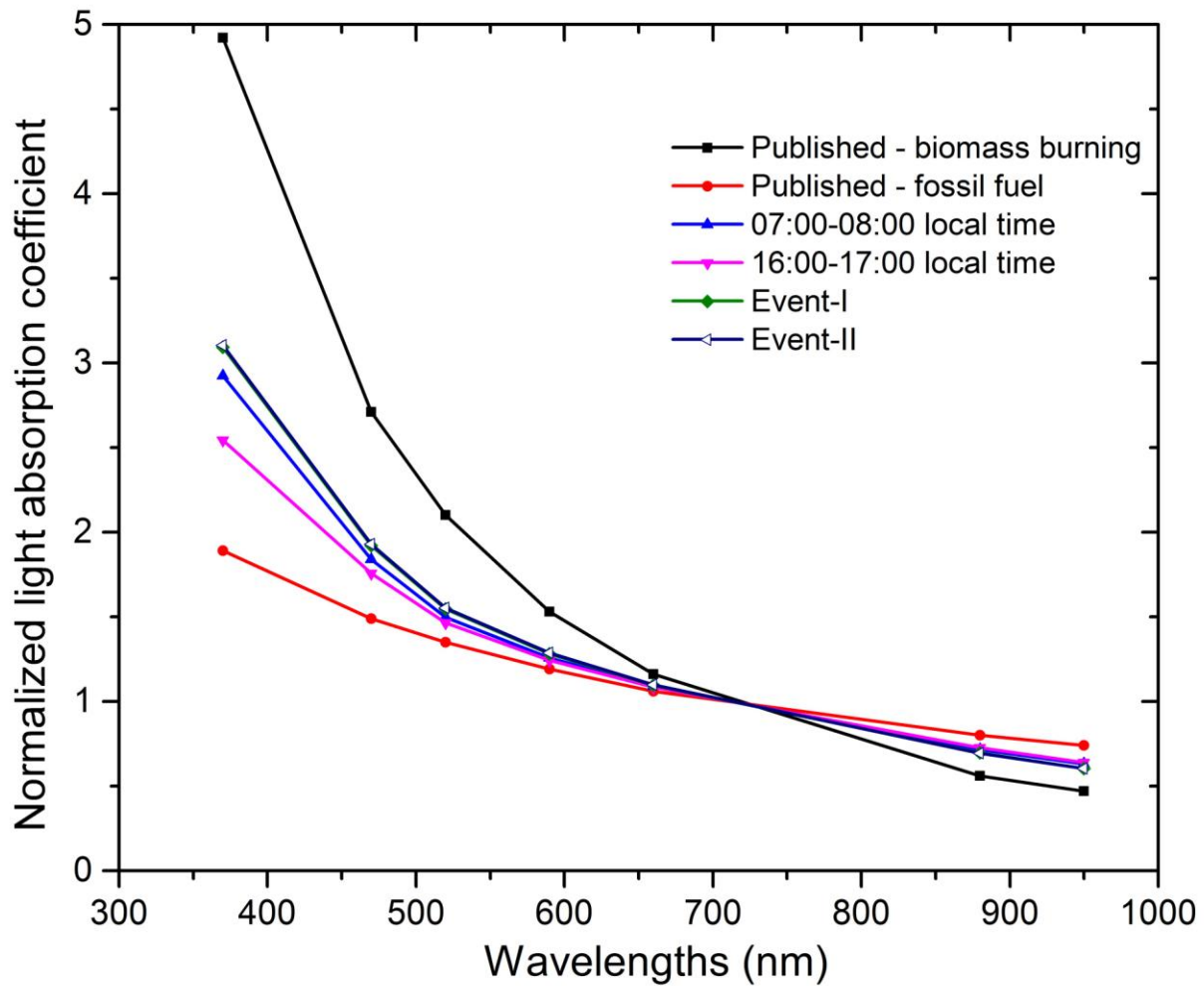
1095



1096

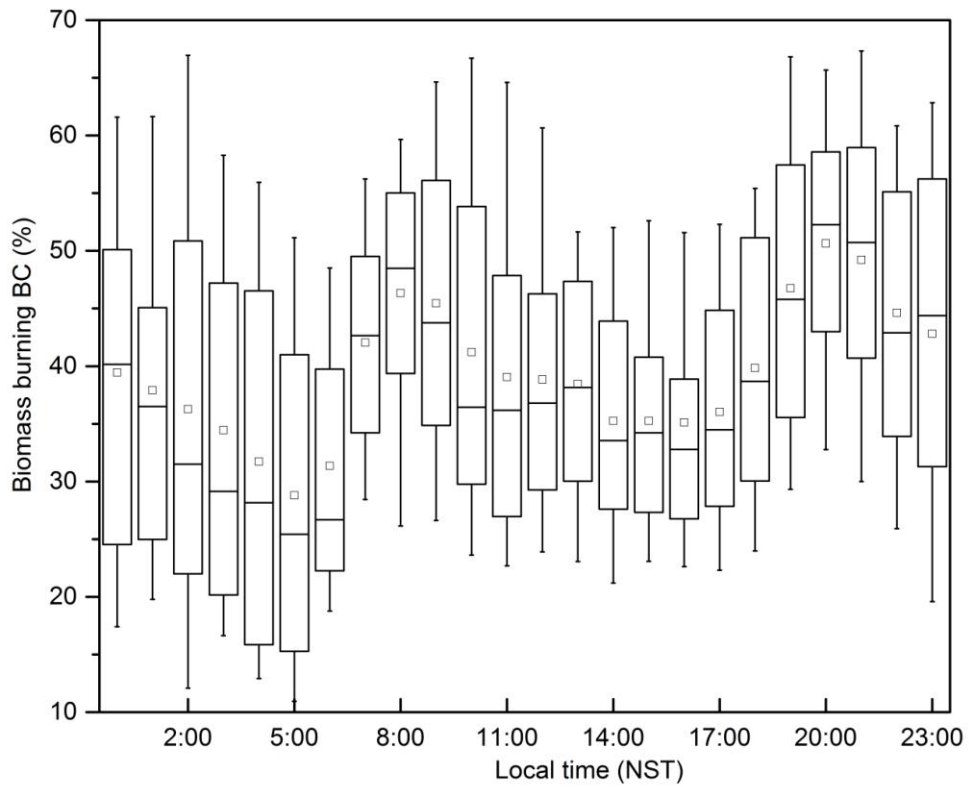
1097 **Figure 10.** (A) WRF-STEM model estimated contributions of various source regions to average
 1098 CO concentration in Lumbini for the sampling period, (B) time series of region tagged CO tracer
 1099 during the whole measurement period using HTAP emission inventory and (C) Figure showing
 1100 percentage increase/decrease in CO concentration with different emissions scenario.

1101



1102

1103 **Figure 11.** Comparison of normalized spectral light absorption coefficients obtained during the
 1104 prime cooking (07:00-08:00 local time) and non cooking time (16:00-17:00 LT) at Lumbini with
 1105 published data from Kirchstetter et al. (2004).



1106

1107 **Figure 12.** Diurnal variation of the fractional contribution of biomass burning to ambient BC
 1108 concentration at Lumbini for the measurement period. In each box, lower and upper boundary of
 1109 the box represent 25th and 75th percentile, respectively, top and bottom of the whisker represents
 1110 90th and 10th percentile, respectively. The mid-line in each box represents median while the
 1111 square mark represents the mean for each hour.

1112